FLIP-MHD: A Particle-in-Cell Method for Magnetohydrodynamics

J. U. Brackbill

CRPC-TR90020
1990

Center for Research on Parallel Computation
Rice University
P.O. Box 1892
Houston, TX 77251-1892

FLIP MHD: A Particle-in-Cell Method for Magnetohydrodynamics

J.U.Brackbill

Group T-3

Los Alamos National Laboratory

January 26, 1990

Subject Classification:

65c20,76w05

Key Words:

adaptive grid, implicit, Lagrangean, magnetohydrodynamics, numerical method, particle-in-cell, time-dependent

Running Head:

FLIP MHD

Mailing Address:

J. U. Brackbill

Group T-3, MS B-216

Los Alamos National Laboratory

Los alamos, NM 87545

I

Abstract

The fluid-implicit-particle-method, FLIP, is extended to magnetohydrodynamic (MHD) flow in two or three dimensions. FLIP-MHD incorporates a Lagrangean representation of the field, and is shown to preserve contact discontinuities, to preserve the Galilean invariance of the MHD flow equations, and to give a grid magnetic Reynolds number up to 16. The conservation of mass, momentum, magnetic flux, and energy are demonstrated by analysis and numerical examples. Results from numerical calculations in two dimensions of the convection of a contact discontinuity, Rayleigh-Taylor unstable flow, and a confined eddy are presented.

I. Introduction

A particle-in-cell (PIC) method, the fluid-implicit-particle-method, FLIP [1], is extended to magnetohydrodynamic (MHD) flow. FLIP-MHD is used to study the effect of hydrodynamic instabilities on magnetic reconnection in the earth's magnetosphere, and similar problems that are dominated by flow at high Reynolds numbers. Such applications require a method with computational diffusion that does not increase with flow speed. Spectral methods have this property, [6], but are less able to model discontinuities and shocks in the flow than are finite-difference methods. For the magnetosphere problem, adaptive zoning is also useful to resolve singularities and to model arbitrary geometries. With FLIP, these capabilities are available for fluid flows, and with FLIP-MHD, these capabilities are extended to magnetofluid flow.

One can place FLIP between "classical" PIC [2], which uses particles to follow the mass motion of the fluid but calculates everything else on a grid, and smoothed-particle-hydrodynamics (SPH), which uses particles but doesn't use a grid at all [3]. In FLIP, particles provide a Lagrangean description of the fluid that resolves contact discontinuities, preserves translational and rotational invariance, and reduces computational diffusion of linear and angular momentum [4, 5]. The interactions among the particles are calculated on a grid for convenience and economy. The present study extends FLIP to MHD, by including

information about the magnetic field among the attributes of the particles.

Monaghan [3] gives a comprehensive review of "particle" MHD methods, which is still current. As he notes, there have been three approaches to "particle" MHD, which we summarize very briefly here.

There is "classical" PIC, with which Butler et al [7] modeled a plasma focus experiment. They applied a specified magnetic pressure to cells in which there were no particles so that a magnetic field entered as an applied pressure boundary condition at the free surface of the plasma.

There are hybrid PIC, finite-difference methods. For example, Brunel et al [8] developed a particle MHD method in which particles represented certain properties of the fluid, while the magnetic field was treated on a grid exactly as in an ordinary finite difference method. The algorithm for solving Faraday's law did not differ significantly from those used in typical finite difference calculations, except in the use of predictor-corrector method to obtain approximate time centering.

There is the grid-free-particle model, the SPH-MHD algorithm, which Monaghan describes [3]. It has been applied with the greatest success to hydrodynamic flow in astrophysical problems. The approximations to the equations of motion in SPH preserve Gallilean and rotational invariance, and do not diffuse angular momentum. Particle interpenetration has been a problem in low

speed flows, which Monaghan has addressed by reformulating the viscosity [22]. In SPH-MHD, the magnetic field is parceled among particles. The evolution of the field is computed particle by particle in the Lagrangean frame of each particle.

The FLIP-MHD method lies between Brunel's and Monaghan's methods. Each particle is assigned data from which the magnetic field is computed each computation step. In this respect, FLIP-MHD is like SPH. However, Faraday's law is solved on a grid each step, and so, in this respect, FLIP-MHD is like Brunel's method. Because the equations on the grid are solved in the Lagrangean frame in FLIP, convection is modeled by the motion of particles through the grid. Particle motion in flow without gradients (in the flow velocity) introduces no computational diffusion, and thus, the method is Galilean invariant. Some computational diffusion is introduced by the assignment of information from the grid to the particles, but the overall diffusion compares favorably with high-order Eulerian, difference methods.

In the following sections, the formulation of FLIP-MHD in two or three space dimensions is described, the algorithm for solving MHD flow problems is outlined, and several computational examples of flow in two dimensions are presented which demonstrate FLIP-MHD's Galilean invariance, and, by comparison with high-order finite-difference approximations to convection, FLIP-MHD's relatively low computational diffusion.

II Resistive Magnetohydrodynamics

Consider, first, the equations for viscous, resistive MHD flow comprising a mass continuity equation,

$$\frac{d\rho}{dt} + \rho \nabla \bullet \mathbf{u} = 0 , \qquad (1)$$

Faraday's and Ampere's laws,

$$\frac{d}{dt}\left[\frac{\mathbf{B}}{\rho} \right] = \frac{\mathbf{B}}{\rho} \bullet \nabla \mathbf{u} + \frac{1}{\rho}\left[\nabla \times \eta \mathbf{J} \right],$$

$$\frac{4\pi \mathbf{J}}{c} = \nabla \times \mathbf{B} , \qquad (2)$$

a momentum equation,

$$\rho \frac{d\mathbf{u}}{dt} = -\nabla \left[p + \frac{\mathbf{B}^2}{8\pi} \right] + \left[\nabla \bullet \frac{\mathbf{BB}}{4\pi} \right] + \nabla \lambda \rho \nabla \bullet \mathbf{u} - \nabla \bullet \mu \rho \Pi \qquad (3)$$

and an energy equation,

$$\rho \frac{dI}{dt} = -p \nabla \bullet \mathbf{u} + \lambda \rho (\nabla \bullet \mathbf{u})^2 + \mu \rho (\Pi \bullet \Pi) + \eta (\mathbf{J} \bullet \mathbf{J}), \qquad (4)$$

ρ is the mass density, $\mathbf{B}$ is the magnetic field intensity, $\mathbf{J}$ is the current density, c is the speed of light, $\mathbf{u}$ is the fluid velocity, I is the specific internal energy, and p is the fluid pressure. The symmetric rate-of-strain tensor, Π is defined in the usual way,

$$\Pi = \frac{1}{2}\left[\nabla \mathbf{u} + \nabla \mathbf{u}^T \right]. \qquad (4a)$$

The pressure is given by an equation of state, $p=p(\rho, I)$.

The transport coefficients are the kinematic shear viscosity

μ, the kinematic bulk viscosity λ, and the resistive diffusivity η. The solenoidal condition on **B**,

$$\nabla \cdot \mathbf{B} = 0, \qquad (5)$$

is assumed as an initial condition. It is important that this property be preserved if the interaction of the field and the plasma be represented accurately. Otherwise, there will develop non-physical, accelerated motion parallel to the magnetic field [9].

Eqs. 1-5, which describe the interaction of an ionized, collisional plasma with a magnetic field, compose the resistive MHD model.

III FLIP Magnetohydrodynamics

To model MHD flow using a particle-in-cell method one must represent the fluid and the field by assigning appropriate properties to particles. The choice that is made in FLIP is discussed below.

A. The FLIP-MHD Algorithm

To solve magnetohydrodynamic flow problems using the particle-in-cell method requires the same 4 steps as for ordinary fluid flow:

Lagrangean phase:

*1. Interpolate the particle data on to a grid to initialize the dependent variables ρ, **u**, **B**, and p at*

the grid points. The overlap of finite-sized particles with the cells of the computation mesh determine the allocation of particle properties to the grid points.

2.Solve finite-difference approximations to Eqs. 1-4 to advance the solution one time step, from t to t+Δt.

3.Interpolate the solutions of the MHD equations on the grid, Eqs. 1-4, to the particles .

Convection phase:

4.Move the grid through the particles to the position it will occupy on the next time step to model convection.

One can compare this algorithm with the arbitrary-Lagrangean-Eulerian (ALE) method for magnetohydrodynamics [13]. An ALE method also separates each computation step into two phases. In the first phase, the finite-difference equations are solved on a Lagrangean grid. In the second phase, convective transport due to relative motion between the grid and the fluid is computed by solving finite difference equations. This phase is the principal source of computational diffusion [5].

In the PIC method, steps 1 and 3 are added to the first phase of the ALE method, and step 4 replaces the second or convective phase. Lagrangean particles replace convective transport, and eliminate one source of computational diffusion. However, Lagrangean particles add another, possible source of computational diffusion in step 3, in which the solutions are transferred from the grid to the particles. This error is discussed in Section IV.

B. The FLIP Particles

In the FLIP code, a particle is assigned a mass, m_p, a momentum, $m_p\mathbf{u}_p$, an internal energy, i_p, and a position, $\mathbf{x}_p$. The interactions among particles are calculated on a grid of arbitrarily-shaped, quadrilateral zones in two dimensions with vertices $\mathbf{x}_{i,j}$, $1\le i\le N_x$, $1\le j\le N_y$. The data for the calculation is the interpolated particle data using a shape or assignment function. To simplify the interpolation when the zones vary in shape and size, each quadrilateral zone is mapped on to a unit square. The mapping in two dimensions corresponds to bilinear interpolation,

$$\mathbf{x}(\xi,\eta) = \xi'\left[(1-\eta')\,\mathbf{x}_{i+1\,j} + \eta'\,\mathbf{x}_{i+1\,j+1} \right] + (1-\xi')\left[(1-\eta')\,\mathbf{x}_{i\,j} + \eta'\,\mathbf{x}_{i\,j+1} \right] \qquad (6)$$

where $\xi'=\xi-i$, $\eta'=\eta-j$, and the mapping is defined for $0\le\xi',\eta',\le 1$.

Note that $\mathbf{x}_{ij}$ maps on to $\xi=i$, $\eta=j$.

C. The Interpolation Equation

The shape function used in FLIP, $S^{(n)}$, is an n-th order B-spline [10]. The use of this shape function in PIC calculations is described in Birdsall and Langdon [11], Hockney and Eastwood [12], and Monaghan [3]. Some of these references interpret the shape function as giving the particle a finite size. In FLIP, this size is defined by the properties of the grid in the neighborhood of the particle in the following way.

Consider the mass contained in a quadrilateral zone denoted by the index c, with centroid $\mathbf{x}_c$ and volume V_c. (The natural coordinates of the centroid are $(\xi',\eta')=(1/2,1/2)$.) The mass is computed using the shape function, $S^{(n)}$, to calculate the overlap of the shape function associated with each particle with the zone, weighted by the mass of the particle. The tensor product interpolation formula that results from evaluating the overlaps in two dimensions is written,

$$m_c = \sum_p m_p \prod_{d=1}^{2} S^{(n)}\left(\xi^d(\mathbf{x}_c) - \xi^d(\mathbf{x}_p) \right), \quad (\xi^1,\xi^2)=(\xi,\eta). \tag{7a}$$

The shape function, $S^{(n)}$, is a positive, symmetric function of the distance in natural coordinates between the two points $\mathbf{x}_c$ and $\mathbf{x}_p$. $S^{(n)}$ has bounded support $(n+1)/2$; when the distance

between two points is greater than (n+1)/2, $S^{(n)}$ is zero. (While the support of $S^{(n)}$ is constant in natural coordinates, it will vary in physical coordinates. Thus, the "size" of a particle is determined by the size of the zones it overlaps.) Further, $S^{(n)}$ is normalized so that,

$$1 = \sum_c \prod_{d=1}^{2} S^{(n)}\left(\xi^d(\mathbf{x}_c) - \xi^d(\mathbf{x}) \right) \tag{7b}$$

for any n and any $\mathbf{x}$ in the domain. That is, the values of $S^{(n)}$ at the grid points form a partition of unity.

To simplify the notation in the following discussion, the interpolation weight given by Eq. (7a) is denoted by,

$$S_{pp'} := \prod_{d=1}^{2} S^{(n)}\left(\xi^d(\mathbf{x}_p) - \xi^d(\mathbf{x}_{p'}) \right). \tag{8}$$

where $\mathbf{x}_p$ and $\mathbf{x}_{p'}$ are any two points on the domain.

D. FLIP-MHD

To extend FLIP to MHD, one assigns a magnetic moment, μ_p, to each particle from which one can calculate a magnetization by interpolation,

$$\boldsymbol{M}_c \, V_c = \sum_p \mu_p \, S_{pc}^{(n)} . \tag{9}$$

The magnetization is usually not solenoidal. If one computes the divergence of $\boldsymbol{M}$ by approximating the derivatives by finite differences and letting the mesh spacing approach zero, there

will remain terms which depend upon the gradient of $S^{(n)}$ that are zero only when $\mathbf{x}_c=\mathbf{x}_p$ or $|\xi(\mathbf{x}_c)-\xi(\mathbf{x}_p)|>(n+1)/2$. Otherwise, the gradient of S is not zero, and the divergence will not be zero.

Because $\boldsymbol{M}$ is not solenoidal, the magnetization cannot be used in place of the magnetic field. If it is used, there results an instability that causes the growth of oscillatory motion in the direction of strong magnetic fields [2]. Since a solenoidal field exerts no force along its own direction, the instability is caused, evidently, by the non-solenoidality of the magnetization.

To initialize a problem, one must specify the magnetization, $\boldsymbol{M}$. In some cases, this is very easy to do. For example, when the magnetic field, $\mathbf{B}$, is uniform as in the examples described below, $\boldsymbol{M}$ and $\mathbf{B}$ are equal. When $\mathbf{B}$ is force-free with current, $\mathbf{J}$, equal to zero, $\boldsymbol{M}$ is zero. However, in some cases the magnetic field corresponds to neither $\boldsymbol{M}$ nor $\mathbf{J}$ equal to zero. In such cases, one must solve for $\boldsymbol{M}$ from the identity,

$$\nabla\times\boldsymbol{M} = \nabla\times\mathbf{B}. \tag{10}$$

That is, the current, $\mathbf{J}$, is the data from which the magnetization, $\boldsymbol{M}$, is initialized.

1. Magnetization and the magnetic field

One can calculate a solenoidal magnetic field from the magnetization by subtracting the gradient of a scalar potential,

$$\mathbf{B} = \boldsymbol{M} - \nabla\phi \tag{11}$$

where ϕ is given by,

$$\nabla \cdot \boldsymbol{M} = \nabla^2 \phi \tag{12}$$

The resulting **B** is solenoidal.

The advantage of using the magnetic moment as a particle variable and calculating a solenoidal magnetic field by projection is that one is required to solve just one potential equation, whether the problem is in two space dimensions or in three. While examples are given for flow in two space dimensions only, the same formulation can be used to solve problems in three dimensions.

Using the relationship between the magnetic field and the magnetization, Eq. (11), one can write the magnetic field energy integral,

$$E_B = \int dV \, \frac{1}{2} \left[\boldsymbol{M} - \nabla \phi \right] \cdot \mathbf{B}. \tag{13}$$

Applying Gauss's theorem allows the explicit display of the boundary contribution,

$$E = \int dV \, \frac{1}{2} \, \boldsymbol{M} \cdot \mathbf{B} - \oint_s ds \, \frac{1}{2} \mathbf{n} \cdot \mathbf{B} \, \phi . \tag{14}$$

If one imposes the Dirichlet conditions, ϕ=0, the surface integral is of course zero. However, if $\mathbf{n} \cdot \mathbf{B}$ is required to be zero on s (i.e. s is a conductor), one should apply the Neumann conditions, given by,

$$\mathbf{n} \cdot \nabla \phi = \mathbf{n} \cdot \boldsymbol{M} , \tag{15}$$

in solving the potential equation, Eq. (12), for ϕ.

2. Equation of motion for the magnetization

On the grid, one solves one's favorite approximations to the MHD equations for **B**. (The ones that are solved in FLIP-MHD are discussed in Refs. [1,4,13, and 14].) One must then advance the magnetization in time. $\boldsymbol{M}$ and ϕ can evolve separately, provided Eq. (11) is always satisfied. Thus, one can postulate an additional evolution equation either for ϕ or for $\boldsymbol{M}$.

Several considerations guide the choice of the additional equation. For mathematical consistency, ϕ must evolve as a scalar. For economy, the evolution equation for $\boldsymbol{M}$ should be explicit. For accuracy, the equations for $\boldsymbol{M}$ and ϕ should have no terms which depend upon the mean flow velocity, or whose approximation will introduce such dependence. That is, one should avoid introducing convection terms, which typically introduce computational diffusion that depends on the mean flow speed.

One evolution equation for ϕ,

$$\frac{\partial \phi}{\partial t} = 0 , \tag{16}$$

clearly satisfies the constraint that ϕ evolve as a scalar, and

yields an equation for $\boldsymbol{M}$, written,

$$\frac{d\boldsymbol{M}}{dt} = \frac{d\mathbf{B}}{dt} + \nabla \bullet \mathbf{u}\, \nabla \phi . \tag{17}$$

However, the second term in Eq. (17) requires evaluating a convection-like term, with all the attendant problems. For this reason, Eq.(16) is discarded.

For plausibility, one should be able to identify some limit in which the equations give an intuitively correct physical result. One can guess the correct physical result for a single particle. ϕ, $\mathbf{B}$, and $\boldsymbol{M}$ should all be constants of the motion, so that,

$$\frac{d\phi}{dt} = 0. \tag{18}$$

Substituting Eq. (18) into the definition of ϕ, Eq. (11), one finds,

$$\frac{d\boldsymbol{M}}{dt} = \frac{d\mathbf{B}}{dt} - (\nabla \mathbf{u}) \bullet \nabla \phi . \tag{19}$$

(A similar equation was derived previously by Fogelson to describe the transport of concentration gradients [24].) In Eq. (19), the second term describes the change in $\nabla\phi$ due to strain. This term depends only on gradients of the velocity, and is unaffected by changes in the mean flow. If $\mathbf{X}$ denotes the Lagrangean coordinate of an element of the fluid, the term can

be written,

$$\frac{d}{dt}\left[\frac{\partial \phi}{\partial x_i}\right] = \frac{\partial}{\partial x_i}\left[\frac{dX_j}{dt}\right]\frac{\partial \phi}{\partial x_j} \quad . \tag{20}$$

Its numerical evaluation neither requires up-winding as would a transport term, nor does it introduce diffusion.

3. The magnetic moment interpolation equation

At this point in a computation step, one has advanced in time the grid magnetization, but not the particle magnetic moments. To do so, one must derive an evolution equation for the particle magnetic moments.

Differentiating the interpolation equation for the magnetization, Eq. (9) results in an implicit expression for the evolution of μ_p,

$$\frac{d\boldsymbol{M}_c V_c}{dt} = \sum_p \frac{d\mu_p}{dt} S_{pc} \tag{21}$$

$\boldsymbol{M}_C$ in Eqs.(9) and (21) is the average value of $\boldsymbol{M}(\mathbf{x})$ over the control volume, V_C,

$$\boldsymbol{M}_c V_c = \int_{V_c} d\,V\,\boldsymbol{M} \quad , \tag{22}$$

The support of S is defined in the Lagrangean frame as noted in Section B, and thus it satisfies the equation,

$$\frac{dS}{dt} = 0 . \tag{23}$$

(The consequences of this definition are discussed in Ref. [4].)

To calculate μ_p using the interpolation equation, Eq. (21), requires solving as many coupled equations as there are particles. This is judged to be prohibitively expensive. One can define an approximate inverse to Eq.(21), written,

$$\frac{d\mu_p}{dt} = \sum_c \frac{1}{N_c} \frac{d\boldsymbol{M}_c V_c}{dt} S_{pc} \ , \ N_c := \sum_p S_{pc} \ . \qquad (24)$$

The approximate inverse replaces the elements in each row by their average value in that row, similarly to a "lumped" mass matrix in finite element methods. This equation has the virtue that it is simple to solve, and that it preserves global flux.

However, the substitution of Eq. (24) for Eq. (21) has the defect that it introduces some computational diffusion. Because only the changes in the magnetization are projected on to the particle using the approximate inverse, no zeroth order diffusion is introduced and the approximation is consistent when any order B-spline is used, not just nearest-grid-point interpolation (n=0) as in classical PIC.[2] (A different approach to removing the zeroth order diffusion than used in FLIP is described by Nishiguchi and Yabe.[15])

IV. Properties of the FLIP-MHD Model

A. Flux Conservation

The proof that magnetic flux is conserved is trivial. One

simply sums both sides of the approximate inverse, Eq. (24), over p, the particle index, to show that,

$$\sum_p \frac{d\mu_p}{dt} = \sum_c \frac{dM_c V_c}{dt} \quad . \tag{25}$$

Even though flux is conserved globally, there is diffusion of the change in the flux because of the substitution of the approximate inverse for the interpolation equation. Recall that the change in the magnetization is transferred to the particles at the end of each time step by solving the approximate inverse equation, Eq. (24). The change is then transferred back to the grid to continue the calculation for the next time interval. This round-trip of the change in the magnetization from the grid to the particles and back results in the substitution of the result of a double interpolation,

$$\frac{dM_c^1 V_c^1}{dt} = \sum_p \sum_{c'} \frac{1}{N_{c'}} \frac{dM_{c'}^L V_{c'}^L}{dt} S_{pc'} S_{pc} \, , \tag{26}$$

for the grid solution even with a Lagrangean grid. The superscript L denotes the result of the numerical solution on the grid, and the superscript 1 denotes the result of the transfer of this solution from the grid to the particles and back. If one sums both sides of the equation over c and substitutes the normalization of S, Eq. (7b), and the definition of N_C, Eq. (24), one can show that magnetization flux is conserved. However, the substitution replaces each grid value by an average including contributions from all the neighboring grid

points within the support of S. The effect of this averaging is similar to the effect of applying a diffusion operator written in conservation form.[16]

One can estimate the diffusivity in one dimension by placing one particle at the center of each cell. First compute the difference between the double interpolation result and the grid result,

$$\frac{d\boldsymbol{M}_c^1 V_c^1}{dt} - \frac{d\boldsymbol{M}_c^L V_c^L}{dt} = \sum_{c'} \frac{d\boldsymbol{M}_{c'}^L V_{c'}^L}{dt} \frac{1}{N_{c'}} T_{cc'} . \tag{27a}$$

The elements of the transfer matrix, T, are defined by,

$$T_{cc'} = \sum_{p} \left\{ S_{pc} S_{pc'} - S_{pc}\, \delta_{cc'} \right\}, \tag{27b}$$

where $\delta_{cc'}$ is the Kronecker δ function. The elements are easily evaluated for quadratic B-splines, yielding a weighted sum of contributions from neighboring grid points. The contributions, $\boldsymbol{M}_c V_c$, to the sum, when expanded in a Taylor series about the value at x_c, yield the diffusion-like expression,

$$\frac{d\boldsymbol{M}_c^1 V_c^1}{dt} - \frac{d\boldsymbol{M}_c^L V_c^L}{dt} = \frac{\Delta x^2}{16} \frac{\partial^2 \frac{d\boldsymbol{M}_c^L V_c^L}{dt}}{\partial x^2} + O(\Delta x^4), \quad \Delta x := x_{c+1} - x_c . \tag{28}$$

The double interpolation, which occurs once each time interval Δt, introduces an error which corresponds to diffusion of the change in magnetization with diffusivity $\Delta x^2/16\Delta t$. The

achievable grid magnetic Reynolds number, $Re_{magnetic}$, is limited by this numerical diffusion. The limit can be estimated from,

$$Re_{magnetic} = \frac{|\mathbf{u}|\Delta x}{\frac{\Delta x^2}{16\Delta t}} = 16\,C\ , \qquad (29)$$

where $C=|\mathbf{u}|\Delta t/\Delta x$ is the material Courant number. Note that the approximation, Eq. (26), to the evolution equation for the magnetization, Eq. (17), is consistent because it is the rate of change of the magnetization that is being diffused, not the magnetization itself.

This diffusivity does not depend upon the flow velocity. Thus, Galilean invariance is preserved, e.g. the solution is unaffected by the addition of a constant velocity to the fluid motion.

B. Magnetic Energy Conservation

One can identify 3 sources of error in magnetic field energy conservation in FLIP-MHD. There is an error caused by the use of the approximate inverse, Eq. (24), and truncation error in the difference approximation to Eq. (19). These errors contribute to errors in the conservation of energy through steps 2 and 3 of the Lagrangean phase of a computation cycle. There is also a dependence of the magnetic field on the grid that causes an error in step 4, when convection is calculated. Through the

interpolation, Eq. (9), the magnetic field depends upon the number and placement of the grid points. Thus, there is a change in magnetic energy when particles move from cell to cell in step 4.

One can contrast this with the conservation of kinetic energy in FLIP, where the particle kinetic energy, defined by,

$$k_p := \frac{1}{2} m_p \mathbf{u}_p^2 \tag{30a}$$

does not change as the particle moves from cell to cell. The corresponding particle magnetic energy

$$e_p := \frac{1}{2} \mu_p \bullet \sum_c \mathbf{B}_c S_{pc} \quad . \tag{31a}$$

contains contributions from interactions among particles. That is, the energy depends upon the magnetic field strength, which is a grid quantity.

Because of the dependence of the particle magnetic energy on the grid, it is impossible to reduce the energy error to a quadratic form similar to the error term in the kinetic energy in FLIP. A brief review of the analysis of the kinetic energy error in FLIP will indicate why.

Recall the definition of kinetic energy in FLIP

$$K_v := \frac{1}{2} m_v \mathbf{U}_v^2 \tag{30b}$$

The subscript v labels the vertices of the mesh where the velocities are stored in FLIP [1]. The vertex velocity, $\mathbf{U}_v$, is defined by,

$$\mathbf{U}_v = \frac{\sum_p m_p \mathbf{u}_p S_{pv}}{\sum_p m_p S_{pv}} . \qquad (30c)$$

(The sum in the denominator defines the vertex mass, m_v.) The total particle kinetic energy is larger than the grid kinetic energy,

$$\sum_p k_p - \sum_v K_v = \sum_{p,p'} \frac{1}{2} m_p \mathbf{u}_p \cdot \mathbf{u}_{p'} \sum_v \left\{ S_{pv} \delta_{pp'} - S_{pv} S_{p'v} \right\} \geq 0, \quad (32)$$

but the rates of change of the particle and grid kinetic energies are equal,

$$\sum_p \frac{dk_p}{dt} - \sum_v \frac{dK_v}{dt} = \sum_p m_p \mathbf{u}_p \cdot \frac{d\mathbf{u}_p}{dt} - \sum_v m_v \mathbf{U}_v \cdot \frac{d\mathbf{U}_v}{dt} = 0 \quad (33)$$

Evidently, the energy surfaces on which the solution evolves for the particles and the grid remain a constant distance apart for a time step. (There are errors in the total kinetic energy when the time derivatives are approximated by finite differences. These are evaluated in Refs. [1,4].)

By an analogous analysis for the magnetic field, one finds that, in contrast to the kinetic energy, the particle and grid magnetic energies are equal but the rates of change are not. Further, the particle magnetic energy, Eq. (31a) includes contributions from interactions among particles that are absent from the particle kinetic energy.

The grid magnetic energy, which is evaluated by discretizing the magnetic energy integral, Eq. (13),

$$E_c = \frac{1}{2} \boldsymbol{M}_c \bullet \mathbf{B}_c V_c \qquad (31b)$$

can be used to show that the total particle and grid magnetic energies are equal,

$$\sum_p e_p = \sum_p \frac{1}{2} \mu_p \bullet \sum_c \mathbf{B}_c S_{pc} = \sum_c \frac{1}{2} \mathbf{B}_c \bullet \boldsymbol{M}_c V_c = \sum_c E_c \ , \qquad (34)$$

However, the rates of change of the particle and grid magnetic energies are not equal. The difference is calculated from Faraday's law, Eq. (2), the approximate inverse, Eq. (24), and the definitions of the particle and magnetic energies, Eqs. (31a), and (31b). The difference is,

$$\sum_p \frac{de_p}{dt} - \sum_c \frac{dE_c}{dt} = -\frac{1}{2} \sum_c \sum_{c'} \mathbf{B}_c \bullet \frac{1}{N_{c'}} \frac{d\boldsymbol{M}_{c'} V_{c'}}{dt} T_{cc'} \ . \qquad (35)$$

The transfer matrix, T, is defined in Eq. (27b). Because the terms in the sum are a product of the magnetic intensity and the magnetization, the total energy changes for the particles and for the grid are not equal. However, the eigenvalues of the transfer matrix are positive, and lie in the interval 0 to N_C [1,4]. Thus the error in the magnetic energy due to double interpolation is opposite in sign to the change in grid magnetic energy and smaller in magnitude.

The energy error given by Eq. (35) can be added to the particle internal energy, particle by particle, to force conservation of total energy. The addition to the particle internal energy is given by,

$$\frac{di_p}{dt} = \frac{1}{2}\sum_c S_{pc}\,\mathbf{B}_c \bullet \sum_{c'} \frac{\frac{dM_{c'}\,V_{c'}}{dt}}{N_{c'}} \left\{ \delta_{cc'} - S_{pc'} \right\} \qquad (36)$$

The sums over c and c' comprise the cells within the support of the particle. The addition is computed simultaneously with the evaluation of the approximate inverse, Eq. (24).

Conservation of total energy through an entire time step is imposed through step 4 by convecting the sum of particle internal and magnetic energies. At the end of step 3, the particle magnetic energy, Eq. (31a), is added to the particle internal energy, using the value of the magnetic field computed on the grid at the end of step 2. At the beginning of the next time step, i.e. at the end of step 1, the particle magnetic energy is computed using the value of the magnetic field computed by solving Eq. (11). The particle magnetic energy is then subtracted to recover the particle internal energy. Errors in magnetic field energy are thus absorbed by adjustments in the internal energy.

Since the particle internal energy and magnetic energy are conserved as the particles stream through the grid, and kinetic energy is conserved separately, the conservation of total energy is enforced. One difference between FLIP-MHD and Eulerian formulations written in conservation form is that the magnetic and kinetic energies are conserved independently. This avoids a common problem in high-speed flows, where small relative errors in the kinetic energy are large relative to the internal energy,

and can drive the internal energy negative.

The sign of the internal energy correction is same as the sign of the change in $M_C V_C$. A decrease in the magnetic energy results in a decrease in the particle internal energy. In strong magnetic fields or cold fluids, one anticipates that the correction will sometimes drive the internal energy of individual particles negative. This is not observed to happen in the examples below.

IV Results

A. Contact discontinuity

A notable property of the particle-in-cell method is its ability to resolve contact discontinuities, even in highly distorted flows [2]. FLIP-MHD extends this capability to discontinuities in the magnetic field by introducing a Lagrangean representation for the field. A uniform flow problem with a discontinuity in the magnetic field direction illustrates this capability.

The FLIP calculation for magnetohydrodynamic flow in two dimensions is performed on a 10x50 mesh, with equal mesh spacing in x and y and periodic boundary conditions in y, the direction with 50 zones. Initially, the uniformly-flowing, constant-density fluid is in pressure equilibrium, and the magnetic field is equal to $\mathbf{B}=B_0\mathbf{n}_z$ in the lower half of the

domain, and $\mathbf{B}=-B_0\mathbf{n}_z$ in the upper half. The sound speed, a, is 100 times the Alfven speed, $A=B/(4\pi\rho)^{1/2}$, and the Mach number, $M=u/a$ is equal to 0.32.

In Fig. 1, the magnetic field profile in y is plotted at the initial time at an x-coordinate corresponding to 1/3 the mesh width. The profile is a mollified square wave. The mollification is a result of the quadratic interpolation in Eq. (9). In Fig. 2, the magnetic field is plotted at a time corresponding to a fluid displacement twice the height of the mesh. There is no diffusion. Errors in the approximate inverse, Eq. (24), have no effect because the particle magnetic moment is a Lagranean invariant when there are no gradients in the flow velocity in the direction of the magnetic field.

A direct measure of the diffusion is given by the integral of the variation in the magnitude of the field over the domain,

$$\Delta B = \int \frac{\left(|\mathbf{B}(x,y,t)| - |\mathbf{B}(x,y,0)| \right)^2}{|\mathbf{B}(x,y,0)|^2} \, dx\, dy . \qquad (37)$$

Any diffusion causes the variation to increase. The variation is plotted in Fig. 3. (A time of 12.5 problem units corresponds to 2 fluid transit times.) The oscillations in the variation have a period equal to the time for the fluid to move one cell. The variation is greatest when the zero value of the magnetic field lands at the center of a cell, and least when the zero lands at a cell edge. The average value of the variation is constant.

With a non-zero resistivity in Eq. (2), the variation increases in time as shown in Fig. 4. The resistive diffusivity corresponds to grid magnetic Reynolds number (computed similarly to Eq. (29)) of 30, and causes an increase in the variation by 400%. The sensitivity of the results to added diffusion indicates the purely numerical diffusion of contact discontinuities in FLIP-MHD calculations has to be very small or negligible to produce the results in Figs. 1-3, as expected.

B. Rayleigh-Taylor instability

The FLIP-MHD code is verified, first, by comparison with the linear stability theory for the Rayleigh-Taylor instability. On a domain in tow space dimensions with 30x15 zones and periodic boundary conditions in y, a heavy fluid is supported against gravity, which acts in the negative x-direction, by a light fluid. The pressure is initially constant. The potential energy oscillates in time, but this appears to have no effect on the results.

Where ρ_1 and ρ_2 are the densities of the light and heavy fluids, g the gravitational acceleration, and k the wave number of the perturbation of the interface between the two fluids, the growth rate is given by,[23]

$$\frac{\gamma^2}{gk} = \left[\frac{\rho_2 - \rho_1}{\rho_2 + \rho_1} - \frac{A^2 k_{parallel}^2}{gk} \right] \qquad (38)$$

The Alfven number, $A=B/2\pi(\rho_1+\rho_2)$, is defined using the average density at the interface, and $k_{parallel}=\mathbf{k}\cdot\mathbf{B}/B^2$. With $ka/(kg)^{1/2}=458$, $kA/(kg)^{1/2}=0.512$, and Atwood number, $A_t=(\rho_2-\rho_1)/(\rho_2+\rho_1)=0.6$, the results are illustrated in Figs. 5 and 6. In Fig. 5, the particles of the heavy fluid are overlaid on contours of constant magnetic flux or field lines at the initial time. After a time, $kAt=4.67$, the heavy particles have formed a spike, and the field lines have been bent in the process as shown in Fig. 6.

The comparison between theory and computation is summarized in Table I. The predicted and computed growth rates agree within expected error except for the case with $\mathbf{B}=1.89$. This field corresponds to zero growth rate theoretically, but a finite growth rate computationally. It can be shown that truncation error in the spatial differencing is accounted for by replacing k by $k'=\sin(k\Delta x/2)/\Delta x/2$. When k' is substituted for k, the growth rate should be zero for $\mathbf{B}=1.92$. However, even a stronger magnetic field, $\mathbf{B}=1.95$, does not suppress the instability completely. It is as though there were resistive diffusion, in which case one would expect a slowly growing instability with

$|\mathbf{B}|>1.89$.

Suppose the resistivity were due to numerical dissipation. One could estimate the magnitude of this numerical resistivity by imposing a physical resistivity just large enough to double the growth rate of the instability. By computation, the resistivity needed to double the growth rate corresponds to a magnetic Reynolds number approximately equal to 250, and a grid magnetic Reynolds number as defined by Eq. (29), equal to 17. The agreement with the predicted value suggests the source of the resistivity is the diffusion due to the use of the approximate inverse to calculate the particle magnetic moments.

The results of a calculation performed on an Eulerian grid are shown in Fig. 7, and of a calculation performed on an Lagrangean grid in Fig. 8. The calculations are shown at kAt=2.8, just before some of the cells in the Lagrangean grid lose convexity. The changes in the magnetic energy and the growth of the enstrophy, defined by,

$$E = \int [\nabla \times \mathbf{u}]^2 d^2\mathbf{x} \qquad (38)$$

are essentially equal. (The enstrophy is used to calculate the growth rates listed in Table I.) The error in the conservation of the total energy, due to truncation error in the approximation of Eq. (19), is equal to less than 1% of the magnetic energy change. There are small differences between the Lagrangean and Eulerian calculations that are probably accounted for by the distortion of the Lagrangean grid. Note that the

particles do not move from cell to cell in the Lagrangean calculation. The calculation is initialized with 9 particles per cell, and there are the same 9 particles per cell at the end.

C. Confined Eddy

The confined eddy problem, which is suggested by a discussion in Moffatt [19] on the effect of plane, differential rotation on an initially uniform magnetic field, is used to test the Galilean invariance of the FLIP method. If the numerical results depend on the relative motion between the fluid and the grid, it has to be due to numerical error because the Navier-Stokes and the resistive magnetohydrodynamics equations are Galilean invariant. However, finite-difference approximations to them typically are not.

The confined eddy has been studied extensively. Solutions of the kinematic problem show that rigid body rotation of a fluid winds the field into a tight, double spiral in the x-y plane[20]. In the limit of infinite conductivity, the field is completely excluded from the rotating region. When the conductivity is finite, closed loops appear and disappear as flux is destroyed within the rotating region. In general, flux is expelled from flows with closed streamlines.

In fluid dynamics experiments, the flows are more complex than the kinematic case considered by Parker. In experiments on

forced, circular shear layers, the vortex sheet at the surface of the eddy is unstable and forms a line of vortices. Thus, secondary eddies are a prominent feature of the steady, driven flow [21]. Numerical solutions with FLIP of initial value calculations of the confined eddy problem display the nonlinear evolution of the instability from many small, secondary eddies to a few large eddies [5]. (An important result of this earlier study is the demonstation that angular momentum is conserved, and vorticity preserved by FLIP.)

Initial-value calculations of the self-consistent effect of plane differential rotation on an initially uniform field are performed. The field is weak, $A/a=10^{-3}$, and the flow is low-speed, $u/a=0.25$, so that the evolution of the flow should be very similar to the incompressible, unmagnetized case.

The initial velocity for the eddy problem is given by,

$$\mathbf{u} = \begin{bmatrix} \omega \times (\mathbf{r}-\mathbf{r}_0), & |\mathbf{r}-\mathbf{r}_0| \leq R \\ 0, & |\mathbf{r}-\mathbf{r}_0| > 0 \end{bmatrix} \qquad (40)$$

where ω is the angular velocity of the eddy. The center of the eddy is placed at the center of a computational domain with dimensions 4R x 4R.

In Fig.9, the magnetic field lines, (contours of constant vector potential $\mathbf{A}$, where $\mathbf{B}=\nabla \mathrm{X} \mathbf{A}$), on a 50x50 zone mesh with FLIP are shown after 1/2 revolution of the eddy. As determined by the specified viscosity and resistivity, the Reynolds number is

25000 and the magnetic Reynolds number is 125. As in the kinematic case, the motion winds the field into a tight, double spiral. A Kelvin-Helmholtz instability causes secondary eddies to form at the periphery of the eddy. After 1 revolution, shown in Fig.10a, the magnetic field is further expelled from the interior of the eddy, and concentrated at the periphery. Large gradients in the field oppose the motion of the eddy, and islands of closed flux have formed due to dissipation in the calculation.

The particles originally within the eddy are plotted in Fig.11a at the time corresponding to Fig.10a. The particles show the nonlinear evolution of the secondary eddies, as the eddies pair to form large, secondary eddies. The secondary eddies are also visible in the vorticity contour plots, shown in Fig.12a. The secondary eddies also expel the flux, increasing the area within which the field is reduced below its initial value.

FLIP replaces convection by the motion of particles through a computation mesh. The particle motion, and the numerical solution of the flow equations on a Lagrangean grid are invariant under the addition of a constant frame velocity, and so it would appear that FLIP results should be frame independent.

To test the Galilean invariance of FLIP-MHD, the calculation above is repeated with a constant velocity added to the initial fluid velocity. In Fig.13, there are shown the stream lines from

two calculations for the confined eddy problem, the one described above shown in Fig.13a, which was performed in a stationary frame, and the other shown in Fig.13b, which was performed in a moving frame. The frame velocity for the moving frame calculation,

$$u = \frac{\omega L_y}{2\pi}, \tag{40}$$

is chosen so that the eddy moves one period in y, L_y, in one revolution of the eddy. The frame velocity and the velocity of flow in the eddy are of comparable magnitude.

Also in Fig.11b, there are plotted the particles that were inside the eddy initially. There is a the same four-fold symmetry of the particle positions in the moving frame calculation as there is in the stationary frame calculation, Fig.11a, particle by particle, even though there are differences in the positions of individual particles, especially those to the outside of the secondary eddies. There are very small differences between the magnetic fields, Fig.10b compared with Fig.10a, and vorticities, Fig.12b compared with Fig12a, in stationary and moving frames.

Another measure of the difference between the calculations is given by the Ohmic heating rate, defined by,

$$H = \int \eta J^2 dV, \tag{42}$$

Ohmic heating is observed to be greater with lower viscosity and lower resisitvity. When diffusion is less, higher gradients in

the magnetic field develop and more heating results. Conversely, increases in numerical diffusion result in decreases in heating. The heating for the stationary fluid is shown in Fig.14, and the moving fluid in Fig.15. There are differences in detail in the heating rates, but overall the heating is very similar for the two calculations.

In finite difference calculations, the invariance is broken by a velocity dependence introduced in approximating the convective derivative. For example, donor cell convection introduces a numerical diffusion of momentum,

$$\nu = \frac{|u|\Delta x}{2}, \qquad (43)$$

that depends upon the velocity relative to the grid, while Lax-Wendroff introduces a dispersion that depends upon the velocity. Even in more sophisticated limiter methods like van Leer's, which use donor cell advection in regions of strong gradients, the errors depend upon the relative velocity. This velocity dependence means that numerical solutions are different in coordinate systems in constant motion relative to each other, contrary to physics.

For comparison with the FLIP results above, there are shown in Figs.16a and 17b the magnetic field lines and vorticities for a calculation performed with PLUTO in a stationary frame, and in Figs.16b and 17b for a calculation performed in a moving frame. The initial conditions for the FLIP and PLUTO calculations are identical.

In PLUTO, the solution of Faraday's law in the Lagrangean frame is followed by an advection step, which approximates the equation,

$$\frac{\partial}{\partial t}\int_V dV\ \mathbf{B} = -\int_S ds\ \mathbf{n}\bullet\mathbf{B} \qquad (44)$$

where V is the control volume, s its surface, and **n** is the outward-directed, unit normal to the surface.

PLUTO substitutes a finite-difference approximation to convective transport for the particle transport in FLIP. Otherwise, PLUTO and FLIP are identical. The approximation is a generalization of the PPM method [18] to a nonrectilinear mesh by Meltz [17].Since the mesh is rectilinear in the case shown, the method reduces, essentially, to the PPM method.

There is a much greater effect of the frame motion in the Eulerian calculations than there is in the FLIP calculations. The most obvious difference is the loss of symmetry in the moving frame results, Figs.16b and 17b, compared with the stationary frame results, Figs.16a and 17b. One notes that the flow velocity relative to the grid is different on the right and left sides of the domain in the moving frame calculation. On the right side, where eddy and frame velocities add, the relative motion between the fluid and the grid is much greater than on the left side, where eddy and frame velocities subtract. The differences between the right and left sides in Figs.16b and 17b are evidence of a velocity dependence in the Eulerian

calculation that is absent in the FLIP calculation. With less accurate finite-difference advection schemes, the loss of symmetry is even more obvious.

What kind of error can there be in the FLIP calculations that causes a difference between stationary and moving frame calculations, yet is independent of the velocity? Consider repeating the stationary FLIP calculation with the grid shifted by a fraction of a mesh spacing. Because the number of particles is finite, the result of projecting the particle data on to the grid, for example the magnetization from Eq. (9), would be different on the shifted grid than on the unshifted grid. Because of small differences in the projected data early in the evolution of the eddy, there would be differences in the subsequent evolution of the eddy because of the instability of the flow. (One would also expect the differences to decrease as the number of particles per cell increases.)

In the moving frame calculation, the motion of the particles through the grid causes their position relative to the grid to be different from the stationary case each time step of the calculation. Thus, the results in the stationary and moving fluid cases are different, even though there is no velocity dependent error. The comparison of the stationary and moving fluid cases demonstrates that the differences are very small.

The velocity dependent errors in the Eulerian calculations also increase the numerical viscosity in the moving frame

calculations. The heating, which is observed in other calculations to increase with increasing Reynolds number, is 50% lower in the moving fluid, shown in Fig. 19, than in the stationary fluid Eulerian calculation, shown in Fig. 18. The heating with FLIP,shown in Figs. 14 and 15, is 10 times as large, and there is no significant difference in the heating in the stationary and moving fluid calculations with FLIP.

V. Discussion

FLIP shares Galilean invariance with several other methods. Pure, grid-free particle methods, like SPH, are frame-independent, as are spectral methods. Compared with SPH, FLIP-MHD is more suitable for bounded flow problems, and, perhaps, is more economical. Compared with spectral methods, FLIP-MHD is better able to represent singularities in the flow, such as shocks and contact discontinuities, expecially if one uses the adaptive grid feature of FLIP.

Since FLIP differs from PLUTO only by the use of particles to model convection, the incremental cost of using particles is measured by difference in execution time on comparable problems. For the confined eddy problem on a 50x50 grid, FLIP requires ~300s, while PLUTO requires ~170s. FLIP execution times are roughly 75% greater. On the other hand, more than twice as many grid points are required to yield the same accuracy with PLUTO as with FLIP in problems with flow, because of the greater

numerical diffusion in the convection phase. In problems without significant flow, for example in equilibrium calculations, PLUTO would give comparable accuracy at lower cost.

Although FLIP's performance is already very good, improved performance would result from finding a better way to evaluate the evolution of the particle magnetic moment, Eq. (21). The approximate inverse, Eq. (24), appears to limit the magnetic Reynolds number that can be modeled and to be the source of dissipation of magnetic field energy.

Acknowledgements

This research was supported by the NASA Office of Space Science and Applications, and by the Institute for Geophysics and Planetary Physics at Los Alamos. Helpful suggestions and criticism by E. Coutsias, J. Friedberg, D. Kothe, P. O'Rourke and D. Sulsky are gratefully acknowledged.

Figures

1. The initial magnetic field profile in y is shown. The domain is periodic in y, with 50 zones in each period. The x-coordinate corresponds to 1/3 the mesh width in x.

2. The magnetic field profile in y is shown after the fluid has traveled twice the length of the mesh in y. There are no visible changes in the profile from the one shown in Fig. (1).

3.The total variation of the magnetic field as calculated from Eq. (27) is shown. The time interval, $0 \leq t \leq 12.5$, is the time required for the fluid to move two periodic intervals in y. The variation, ΔB, oscillates about a mean value that is nearly constant in time.

4. The variation of the field is shown with resistive diffusion. The grid magnetic Reynolds number, Eq. (29), is 30. The variation increases by 400% during 2 fluid transit times.

5. The particles of the heavy fluid (depicted by dots) and magnetic field lines (depicted by lines) illustrate the initial conditions for a calculation of the Rayleigh-Taylor instability.

6. The growth of the Rayleigh-Taylor instability for the initial conditions shown in Fig. 5 causes the heavy-fluid particles (depicted by dots) to form a spike, and to bend the magnetic field lines (depicted by lines) by kAt=4.67.

7. The heavy particles in a Rayleigh-Taylor instability calculation are plotted on the Eulerian computation mesh at kAt=2.8.

8. The heavy particles for a Lagrangean calculation of the same problem as in Fig. 7 are plotted on the Lagrangean computation mesh. The distortion of the mesh illustrates why a Lagrangean mesh is unsuitable for highly distorted flow. Any shear in the flow causes a Lagrangean grid to fail eventually.

9. Magnetic field lines from a FLIP-MHD calculation of the confined eddy are plotted after 1/2 revolution of the eddy. The magnetic Reynolds number is 125.

10. After a full revolution of the eddy, the magnetic field lines calculated with FLIP-MHD form the complex patterns shown. The results in (a), for a stationary fluid, and in (b), for a moving fluid, are similar in symmetry and structure if different in detail.

11. Particles forming the eddy at the inital time in the FLIP-MHD calculation have moved into the pattern of primary and secondary eddies shown after one revolution of the eddy. The particles in (a) and (b) correspond to the magnetic fields in (10a) and (10b) respectively.

12. Contours of constant vorticity calculated by FLIP-MHD are plotted after one rotation of the eddy. The contours in (a) and (b) correspond to the particles in Fig. 11a and 11b respectively.

13. The streamlines calculated by FLIP-MHD after one rotation are plotted in (a), for a stationary fluid, and in (b), for a moving fluid. The contours in (b) clearly show the dominance of

the imposed, uniform flow almost everywhere.

14. The Ohmic heating calculated with FLIP-MHD, defined by Eq.(42), is plotted for the confined eddy in a stationary fluid. The time, t=12.5, is the rotation period for the eddy in problem units.

15. The Ohmic heating is plotted for the confined eddy in a moving fluid. The peak value at t=7.5 is the same as for the stationary fluid, shown in Fig. 14, as is the value at t=12.5.

16. The magnetic field lines calculated with PLUTO for the confined eddy problem are shown at the end of one rotation period. The PLUTO calculations are in a stationary fluid, (a), and in a moving fluid, (b), with the same initial and boundary conditions as for the FLIP-MHD calculations in Figs. 10-15. The loss of symmetry in (b) results form a velocity dependent diffusion in the approximation of convection.

17. The vorticity contours calculated with PLUTO corresponding to Fig. 16 are shown. For a stationary fluid, (a), the PLUTO and FLIP-MHD results, Fig. 12, are similar. For a moving fluid, (b), the symmetry is lost in the PLUTO results.

18. The heating calculated with PLUTO is shown for a stationary fluid. The maximum heating rate is about 10% of the FLIP-MHD rate.

19. The heating calculated with PLUTO is shown for a moving fluid. The peak heating is reduced by 40% from the result for a stationary fluid, Fig. 18.

References

1. J. U. Brackbill and H. M. Ruppel, J. Comput. Phys. 65, 314 (1986).

2. F. H. Harlow, Meth. Comput. Phys. 3, 319 (1963).

3. J. J. Monaghan., Comput. Phys. Repts 3, 71 (1985).

4. J. U. Brackbill et al, Comput. Phys. Commun. 48, 25 (1988).

5. J. U. Brackbill, Comput. Phys. Commun. 47, 1 (1987).

6. David Gottlieb, and Steven A. Orszag, *Numerical Analysis of Spectral Methods*, pp135-141, (Society for Industrial and Applied Mathematics, Philadelphia, 1977).

7. T. D. Butler et al, Phys. Fluids 12, 1904 (1969).

8. F. Brunel et al, J. Comput. Phys. 43, 268 (1981).

9. J. U. Brackbill and D. C. Barnes, J.Comput.Phys. 35, 426 (1980).

10. Carl deBoor, *A Practical Guide to Splines*, (Springer-Verlag, New York,1978).

11. Charles K.Birdsall and A. Bruce Langdon, *Plasma Physics via Computer Simulation*, (McGraw-Hill, New York, 1985).

12. R. W. Hockney and J. W. Eastwood, *Computer Simulation Using Particles*, (McGraw-Hill, New York, 1981).

13. J. U. Brackbill, Meth. Comput. Phys. 16, 1 (1976).

14. J. U. Brackbill, "Fundamentals of numerical

magnetohydrodynamics" in *Proc. 3rd International School for Space Simulation*, edited by B. Lembege, (Cepadues-Editions, Toulouse, 1989), p183.

15. A. Nishiguchi and T. Yabe, J. Comput. Phys. 52, 390 (1983).
16. James W. Eastwood, Comput. Phys. Commun., 48, 17 (1988).
17. Meltz, Bertrand J. A., J. Comput. Phys., submitted.
18. P. Colella and P. Woodward, J. Comput. Phys., 54, 115 (1984).
19. H. K. Moffatt, *Magnetic field generation in electrically conducting fluids*, (Cambridge University Press, New York, 1978).
20. R. L. Parker, Proc. Roy. Soc. A291, 60 (1966).
21. J. M. Chomaz, et al, J. Fluid Mech. 187, 115 (1986).
22. J. J. Monaghan, J. Comput. Phys. 82, 1 (1989).
23. S. Chandrasekhar, *Hydrodynamic and Hydromagnetic Stability*, (Dover Publications, New York, 1961).
24. A. L. Fogelson, Department of Mathematics, University of Utah, private communication.

Table I

Comparison of theoretical and computed growth rates for the Rayleigh-Taylor instability

Magnetic field strength-$(kA)^2/kg$	Theoretical growth rate - $\gamma/(kg)^{1/2}$	Computed growth rate- $\gamma/(kg)^{1/2}$
0.0	0.774	0.76
0.1675	0.656	0.61
0.60	0.0852*	0.098
0.62	0.0	0.072

* with k' replacing k in Eq. (38)

Fig 1

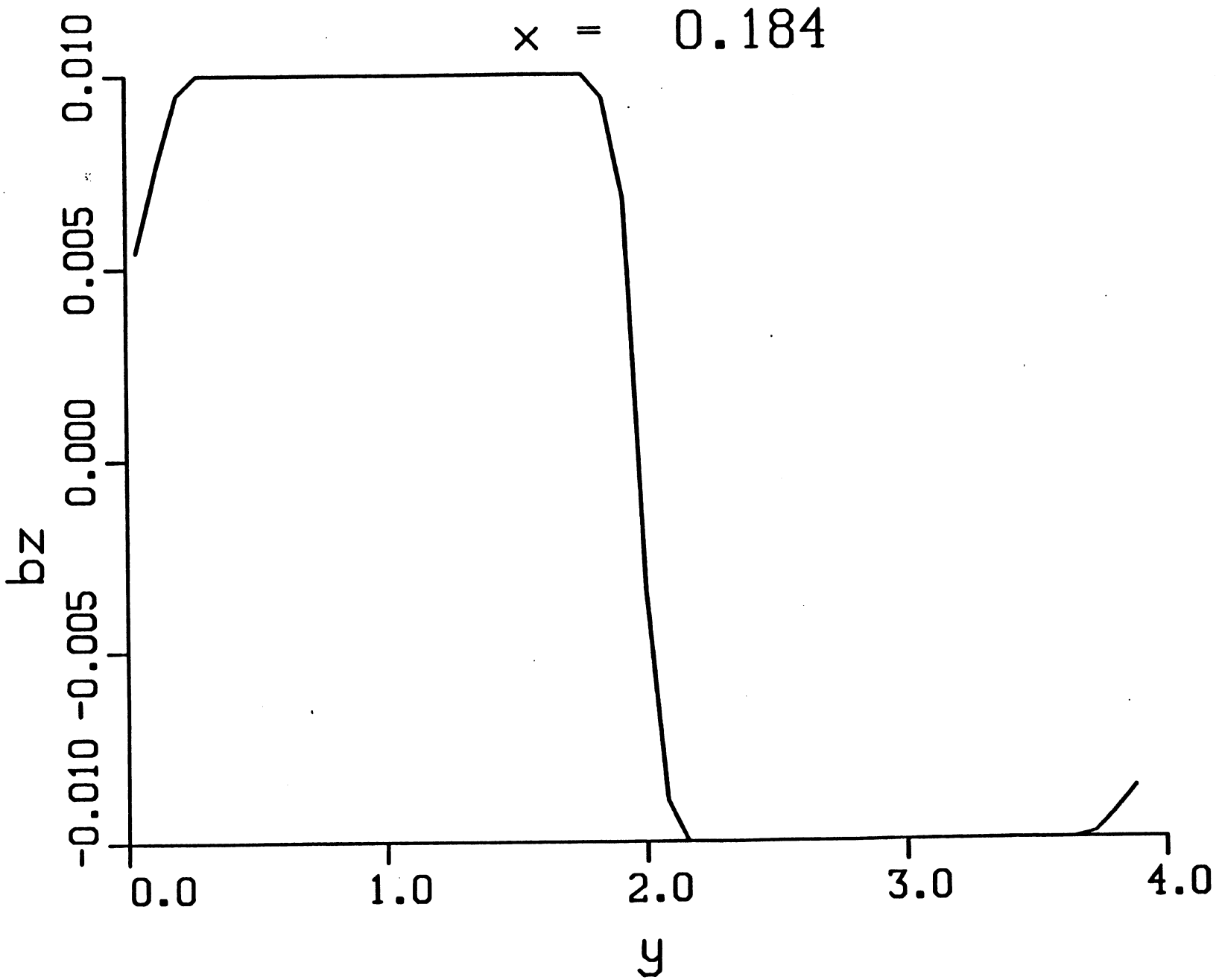

Fig 2

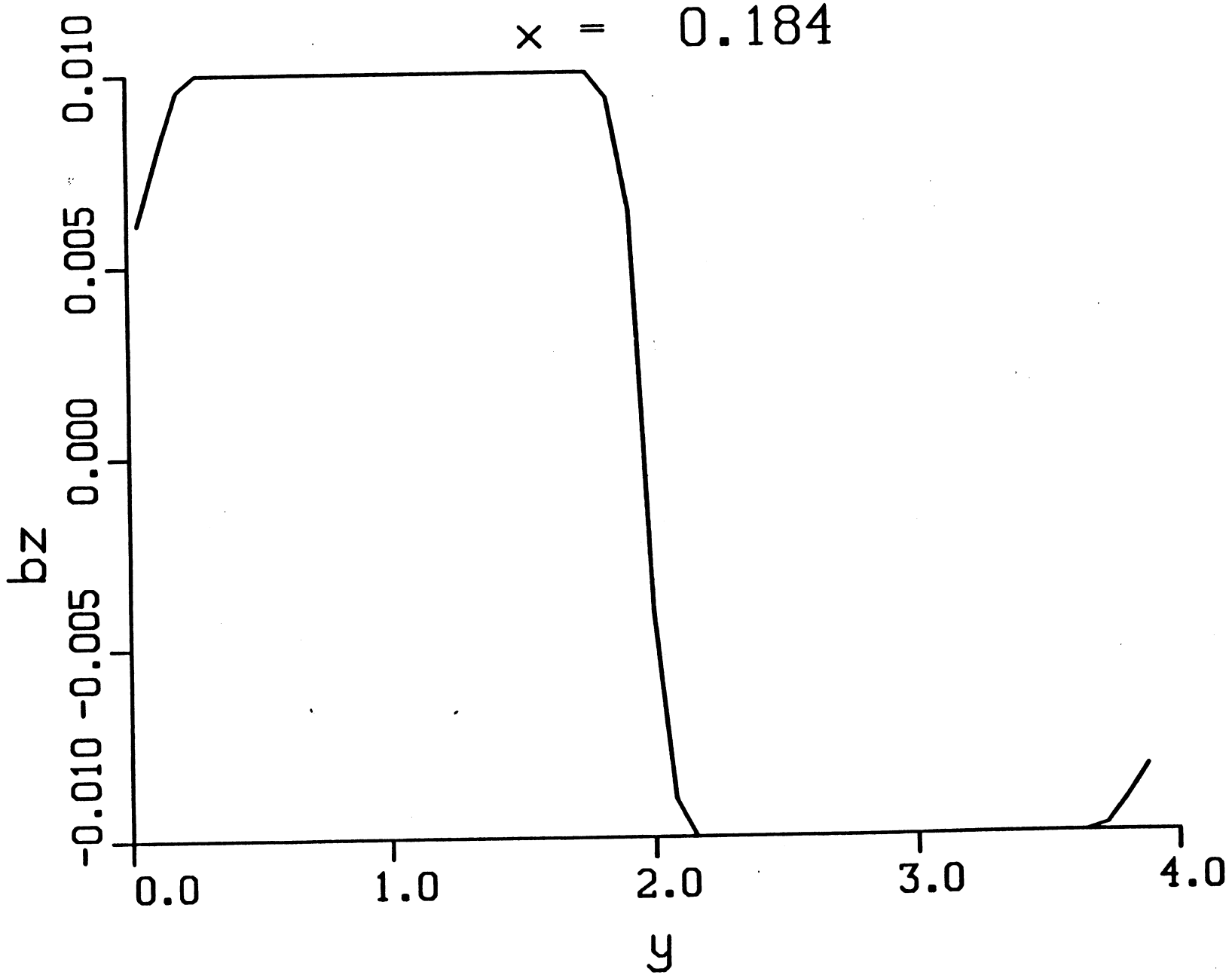

Fig 3

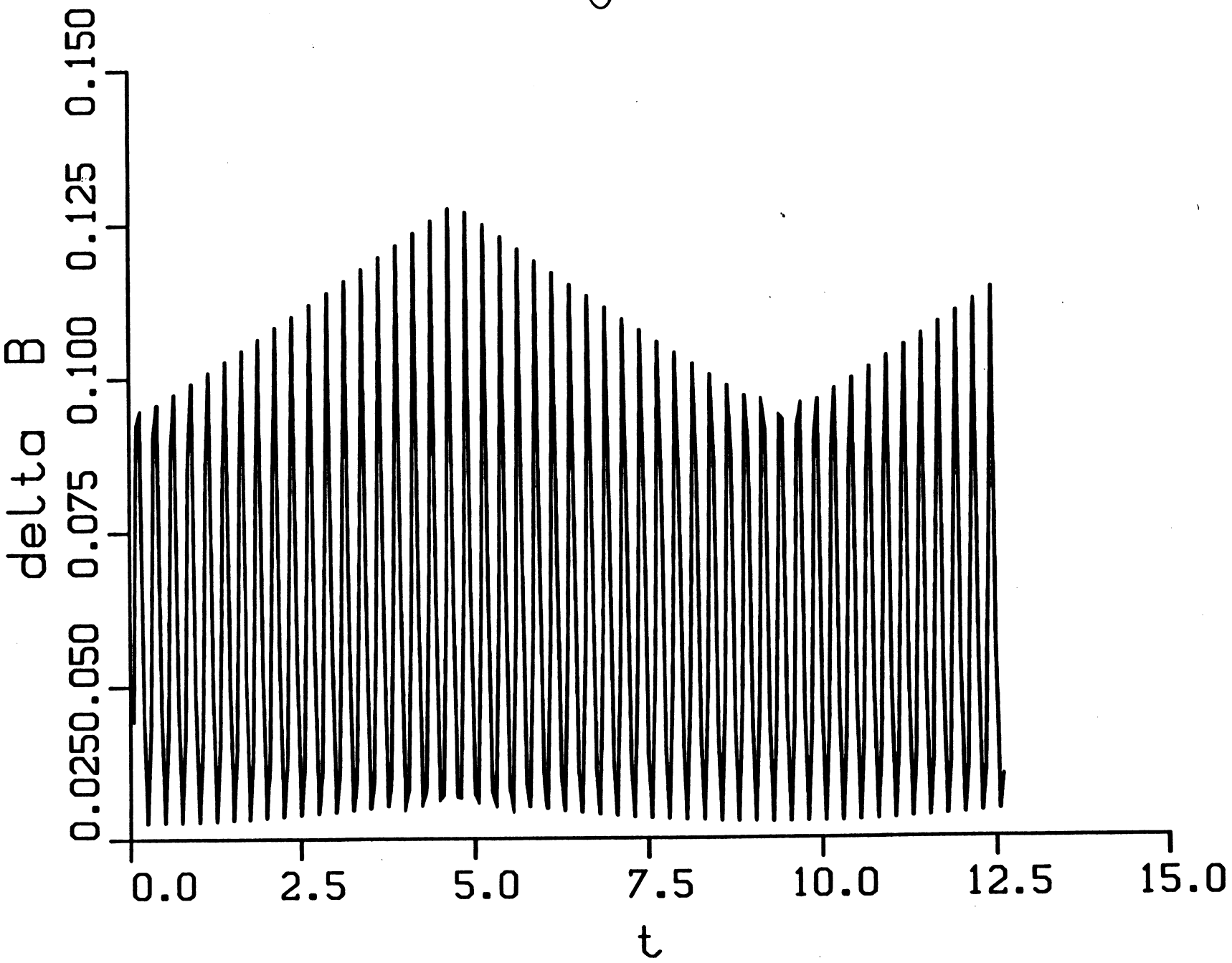

Fig 4

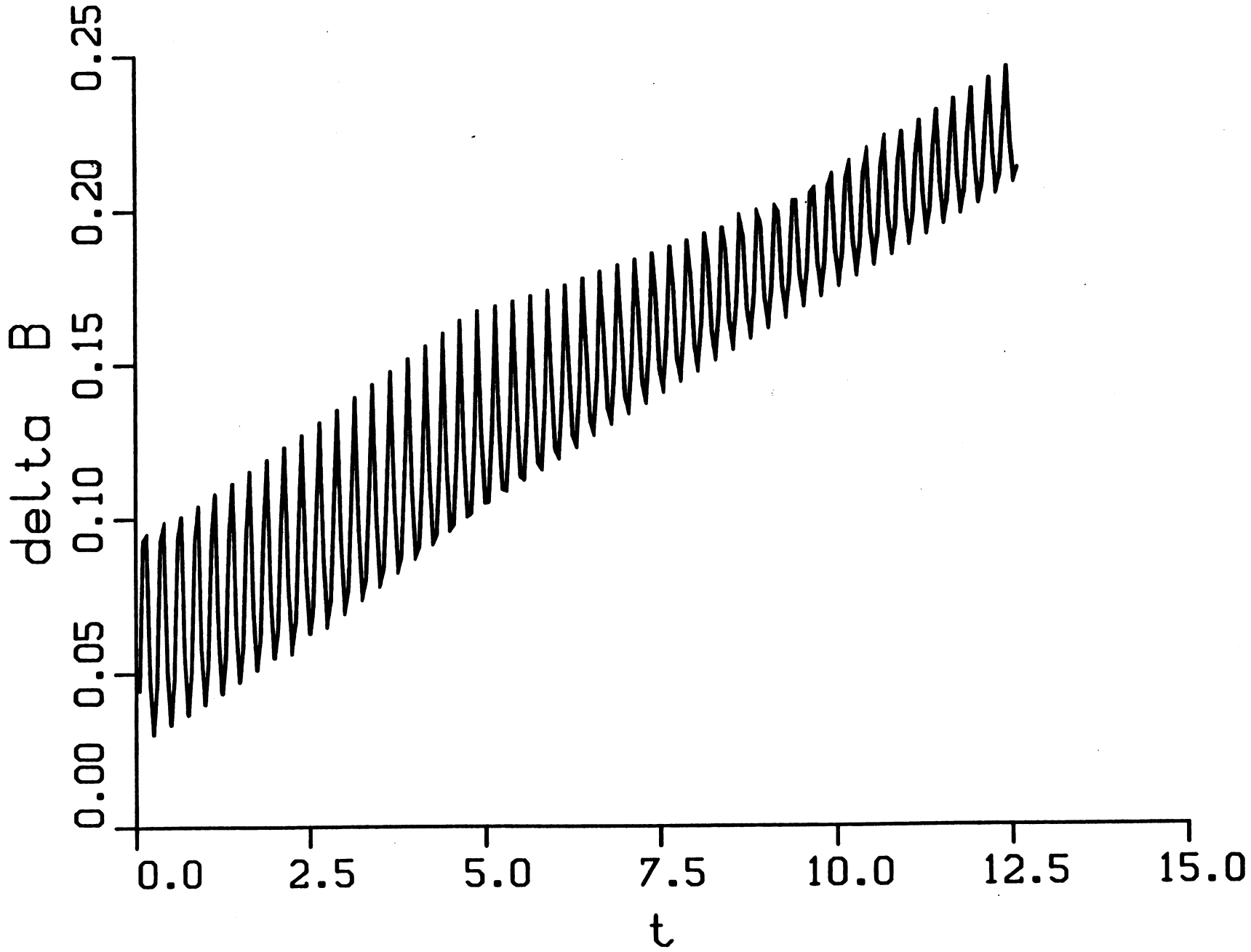

Fig. 5

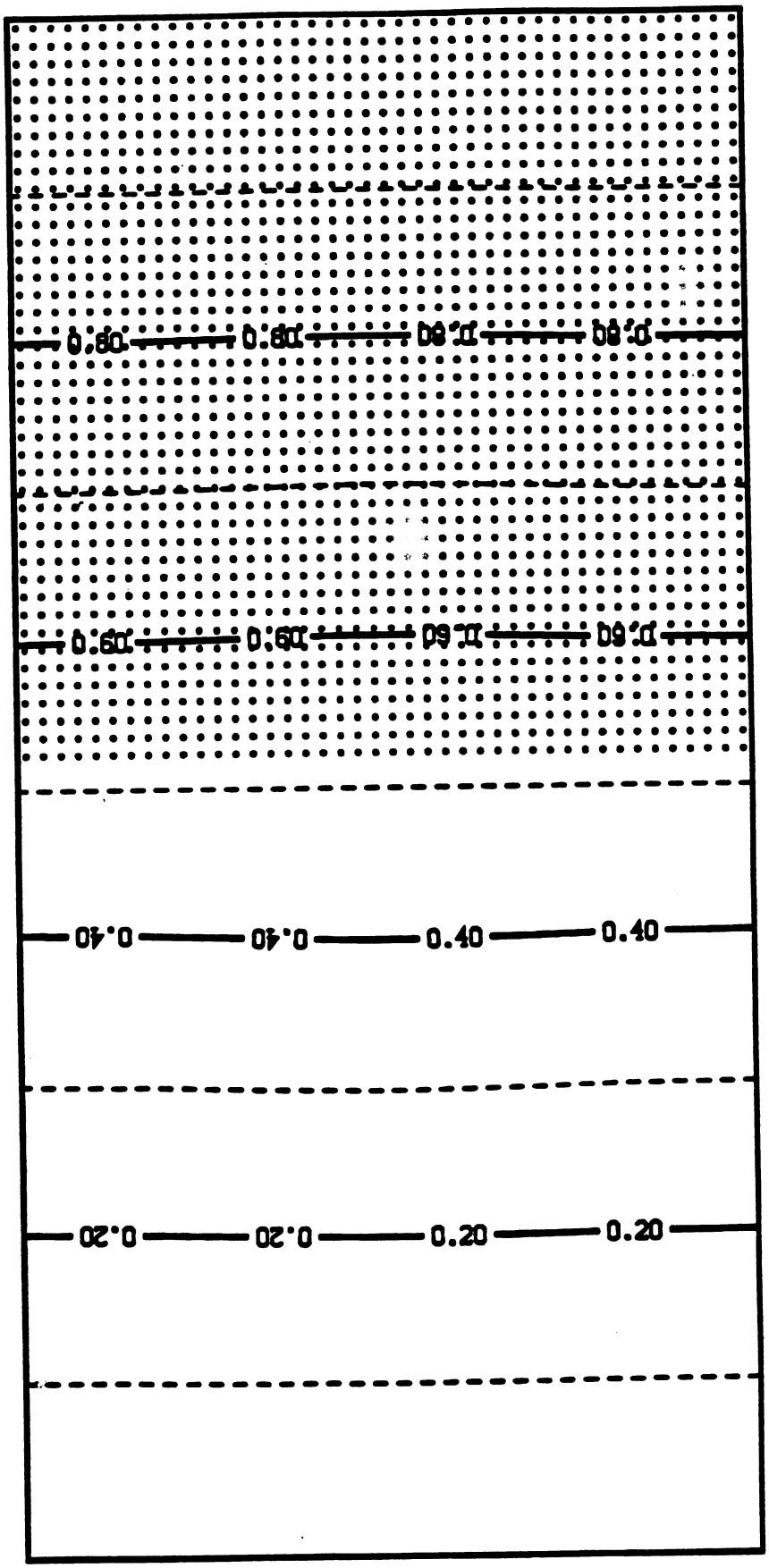

Fig 6

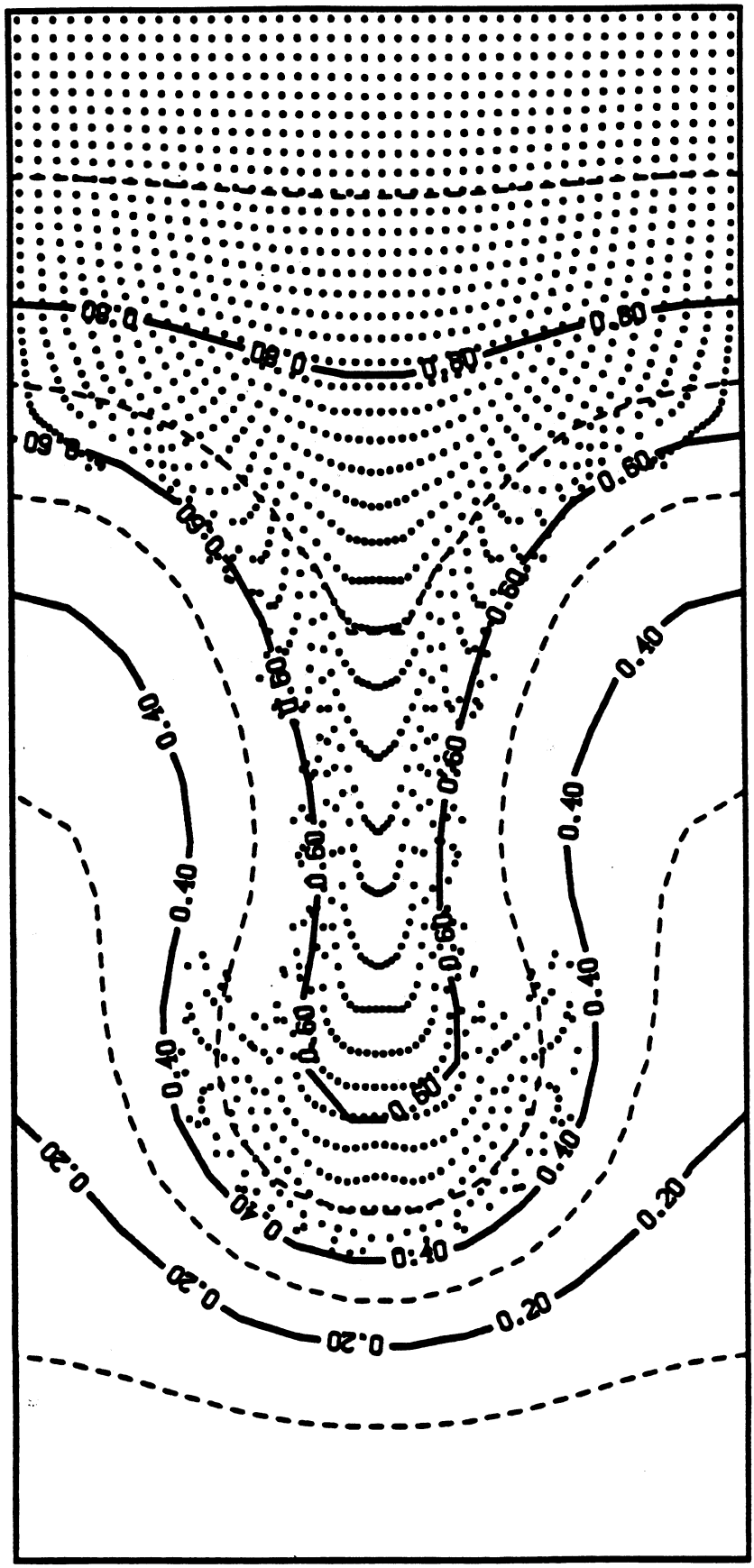

Fig. 7

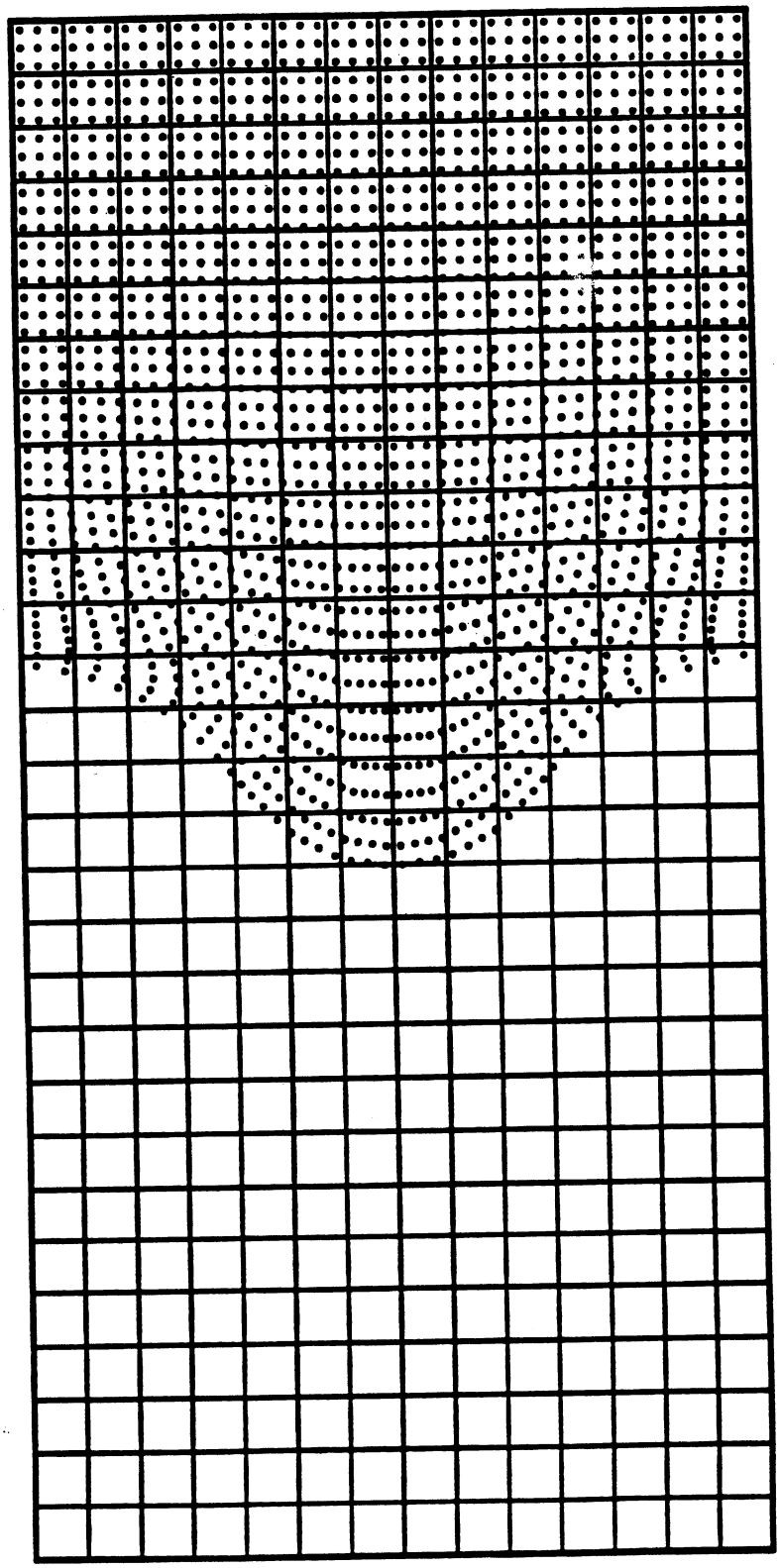

Fig. 8

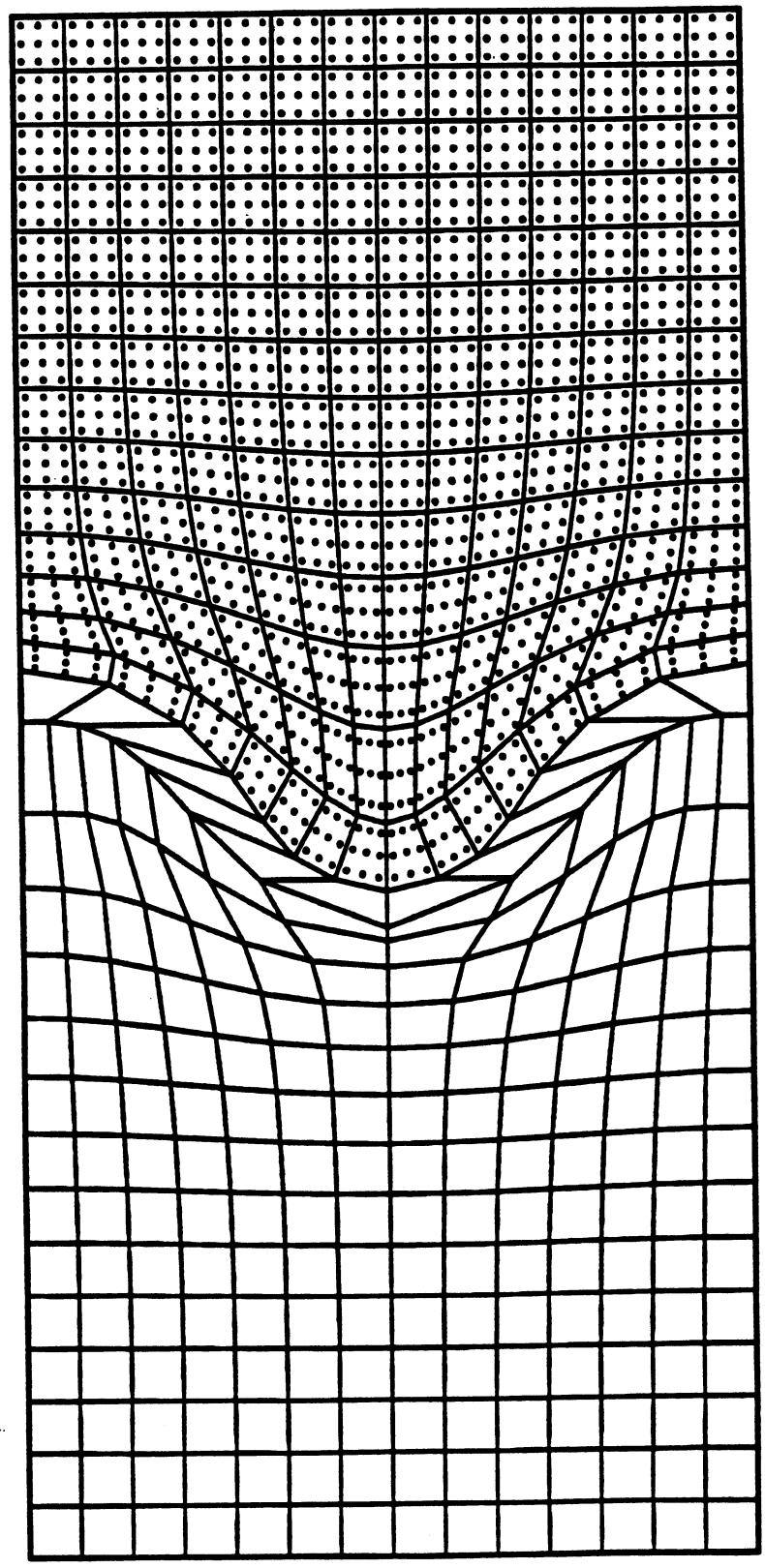

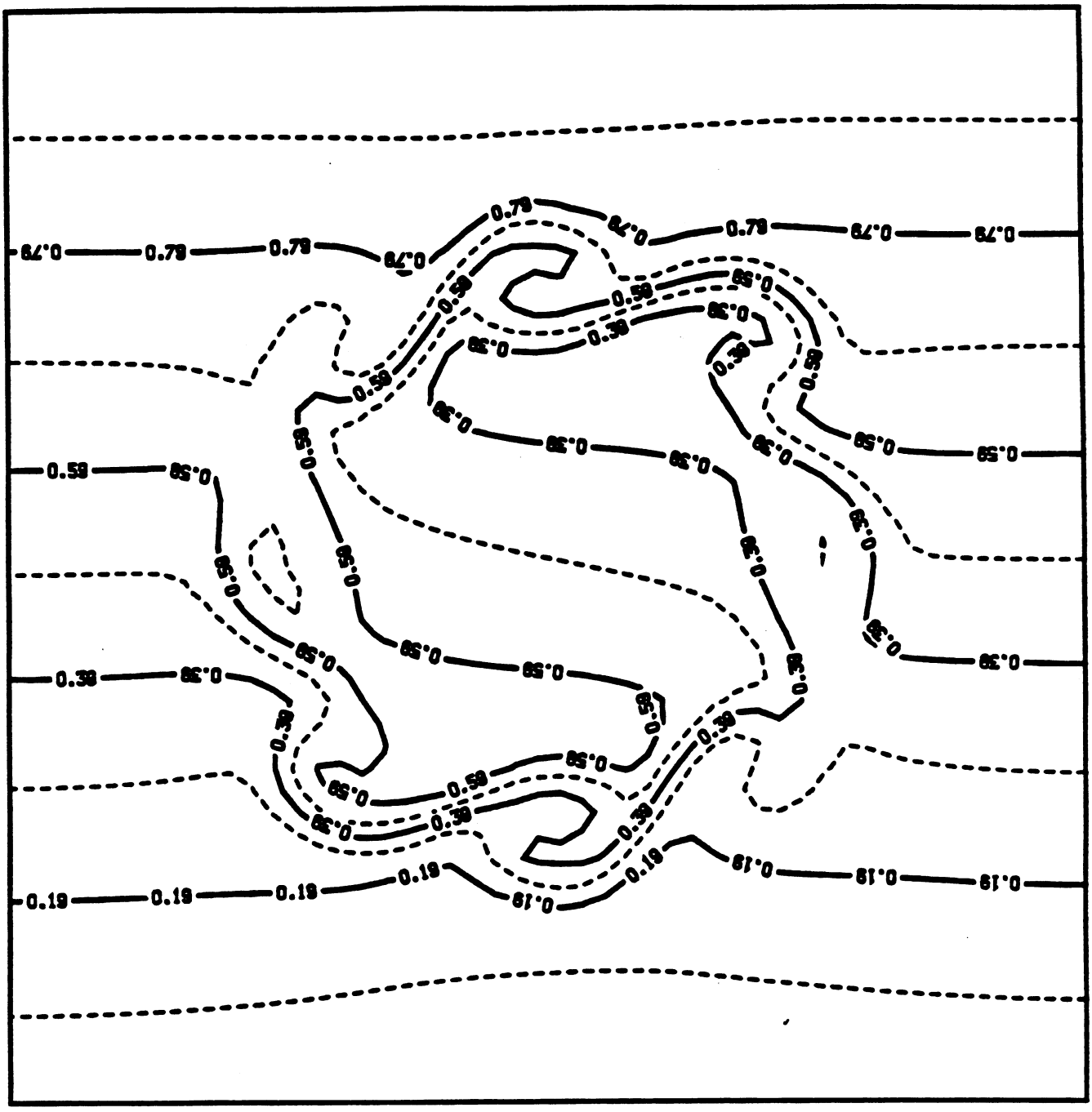

Fig 9

Fig 10

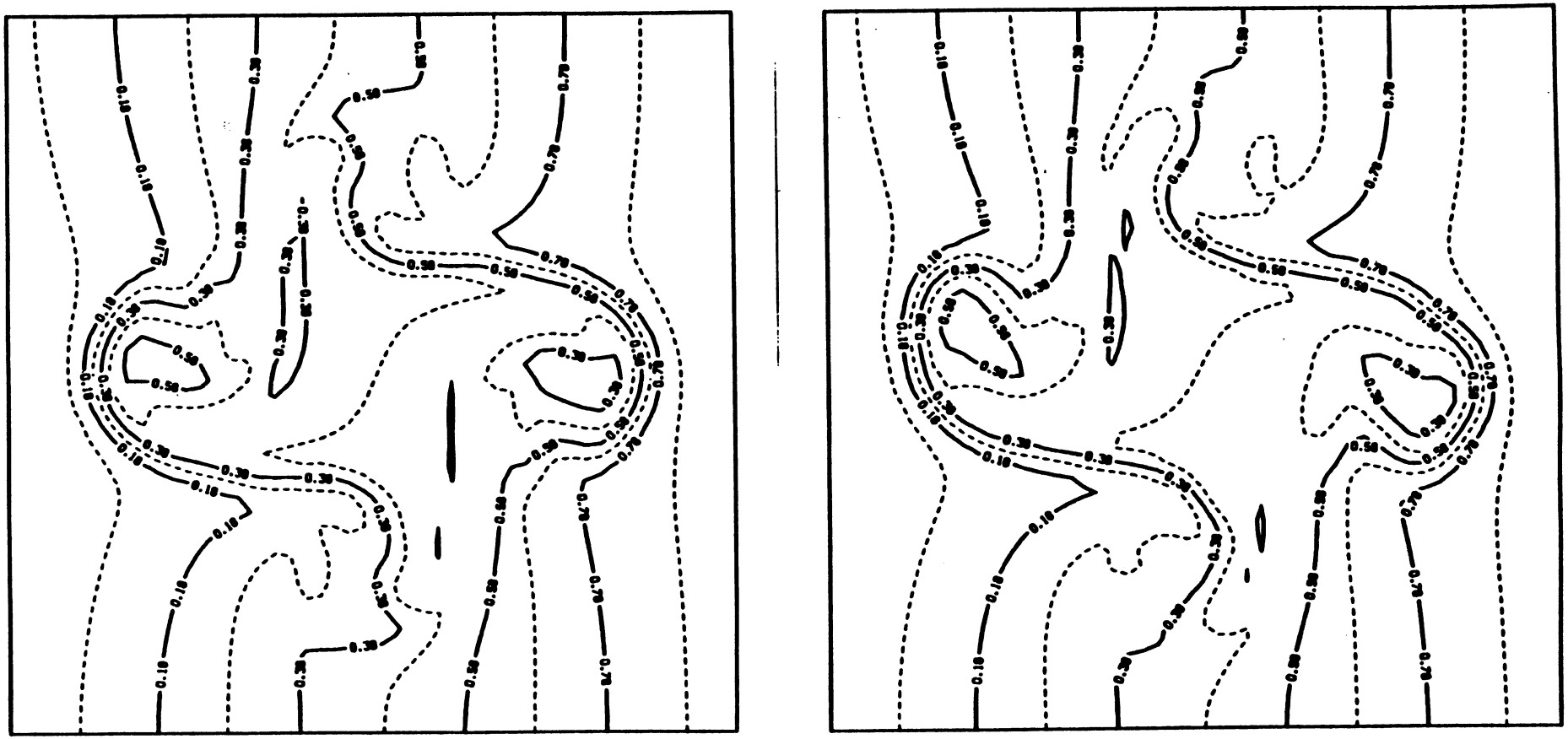

(A) (B)

Fig 11

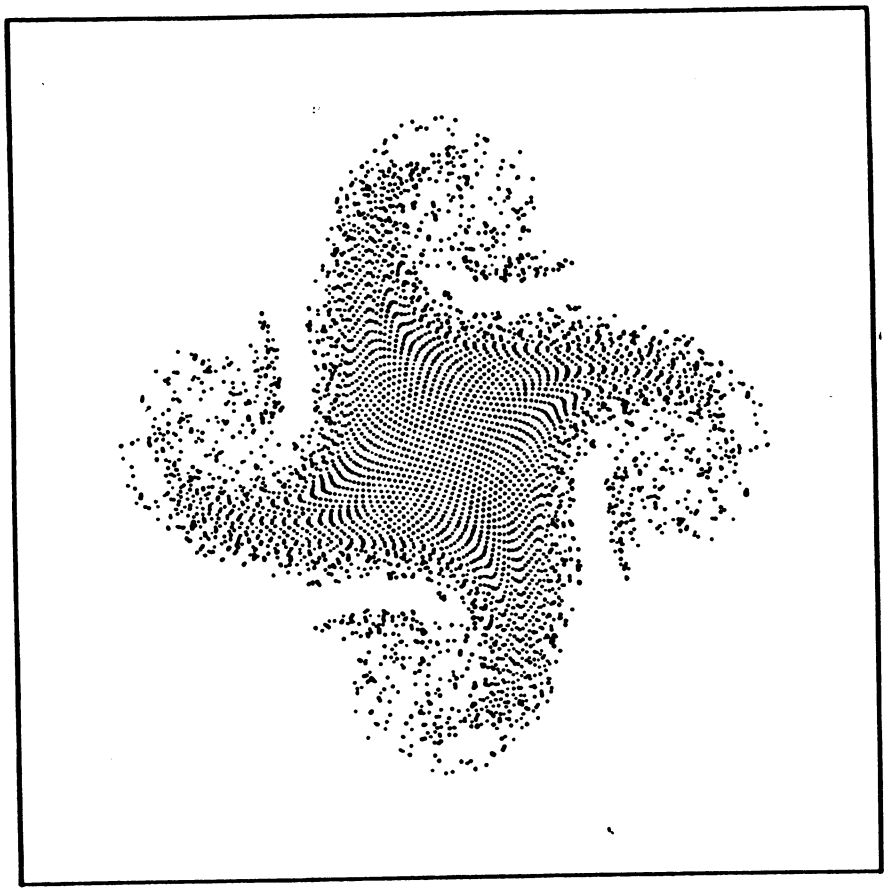

(A)

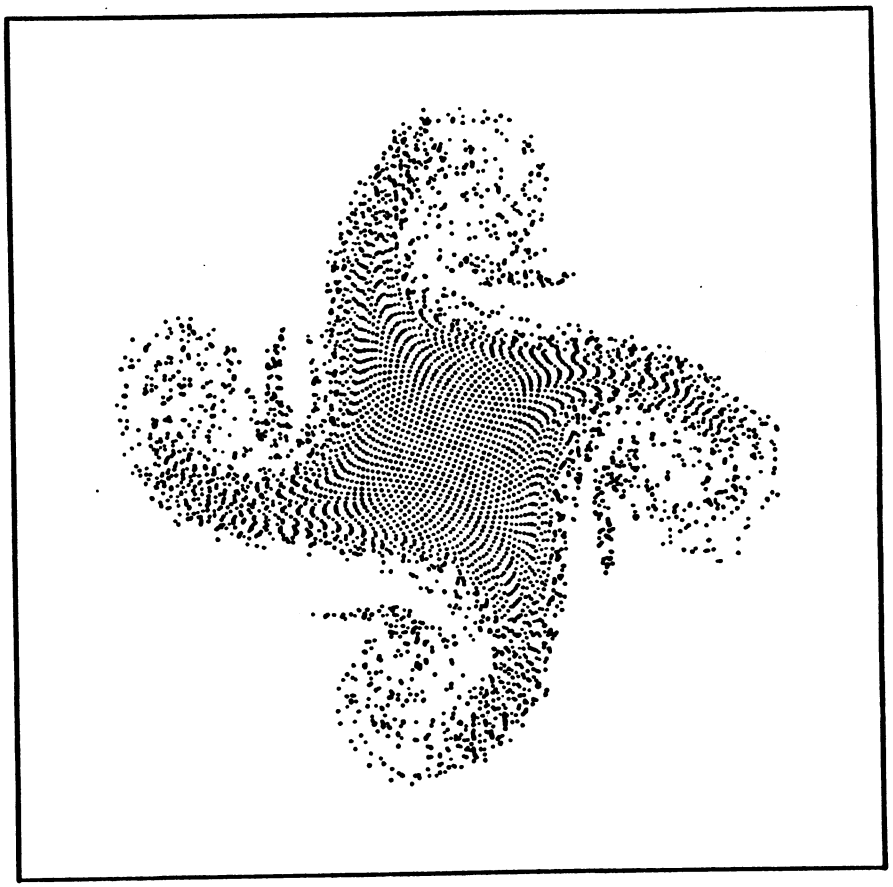

(B)

Fig. 12

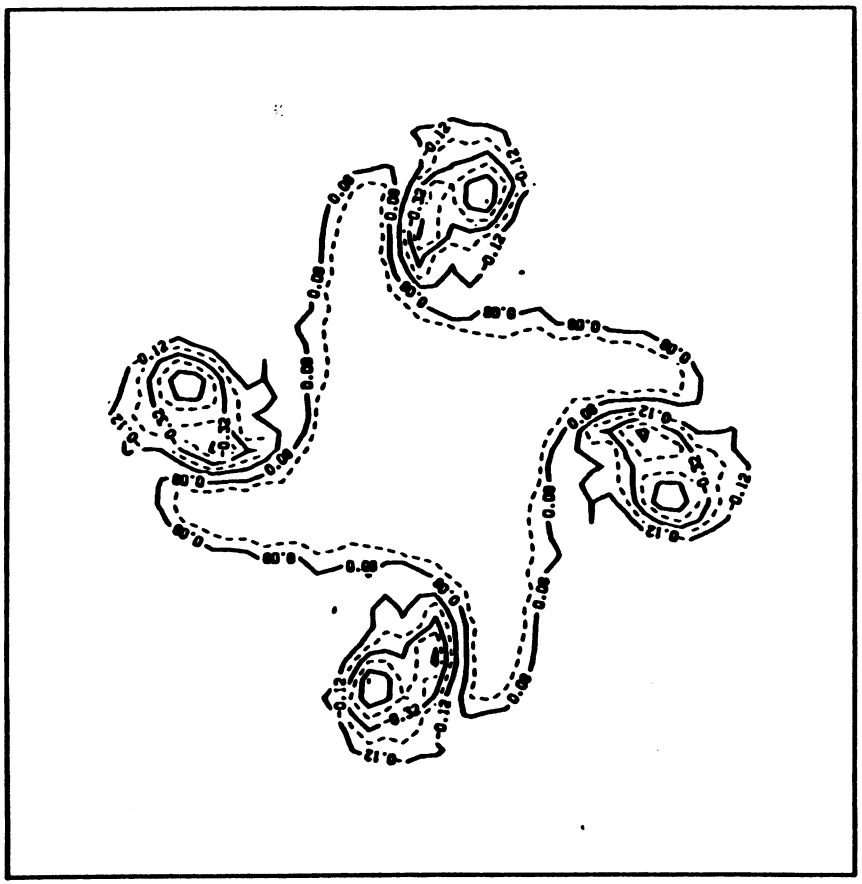

(A)

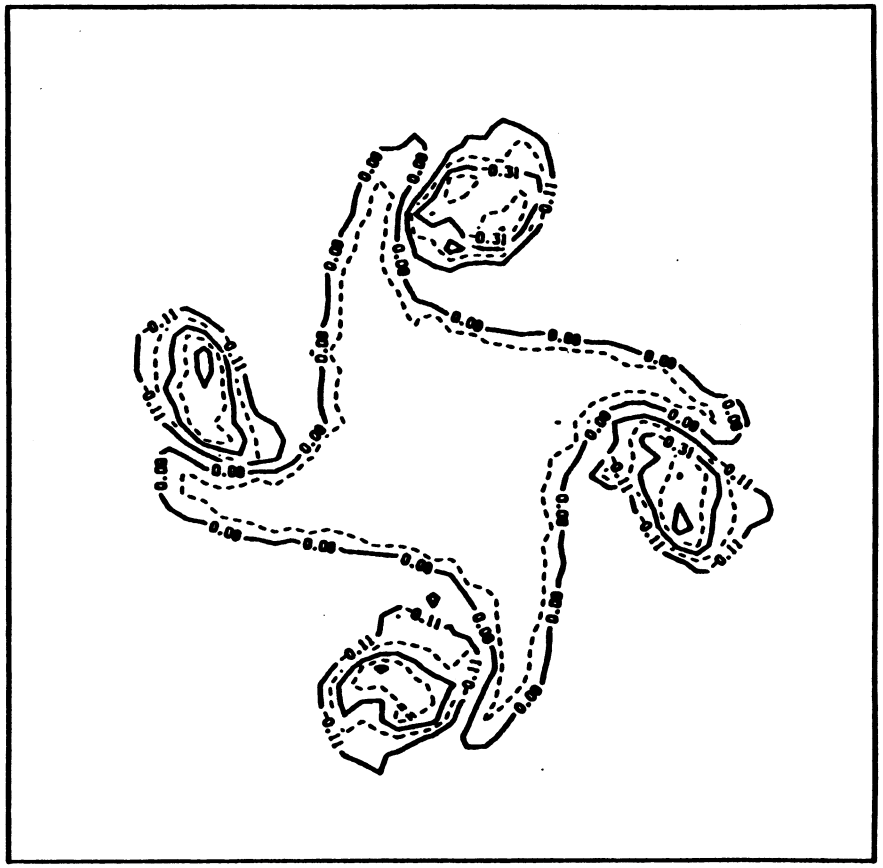

(B)

Fig. 13

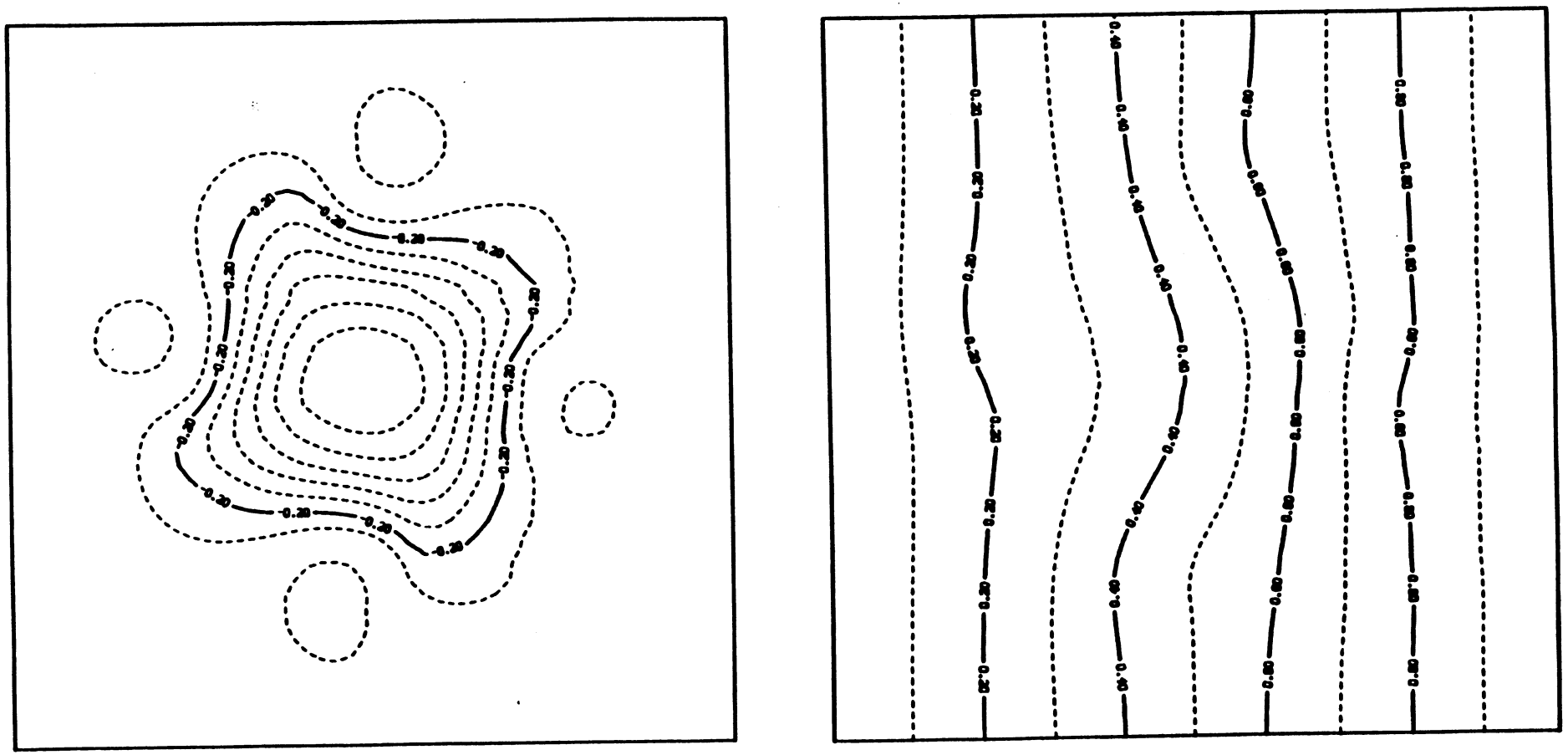

(A)

(B)

Figure 14

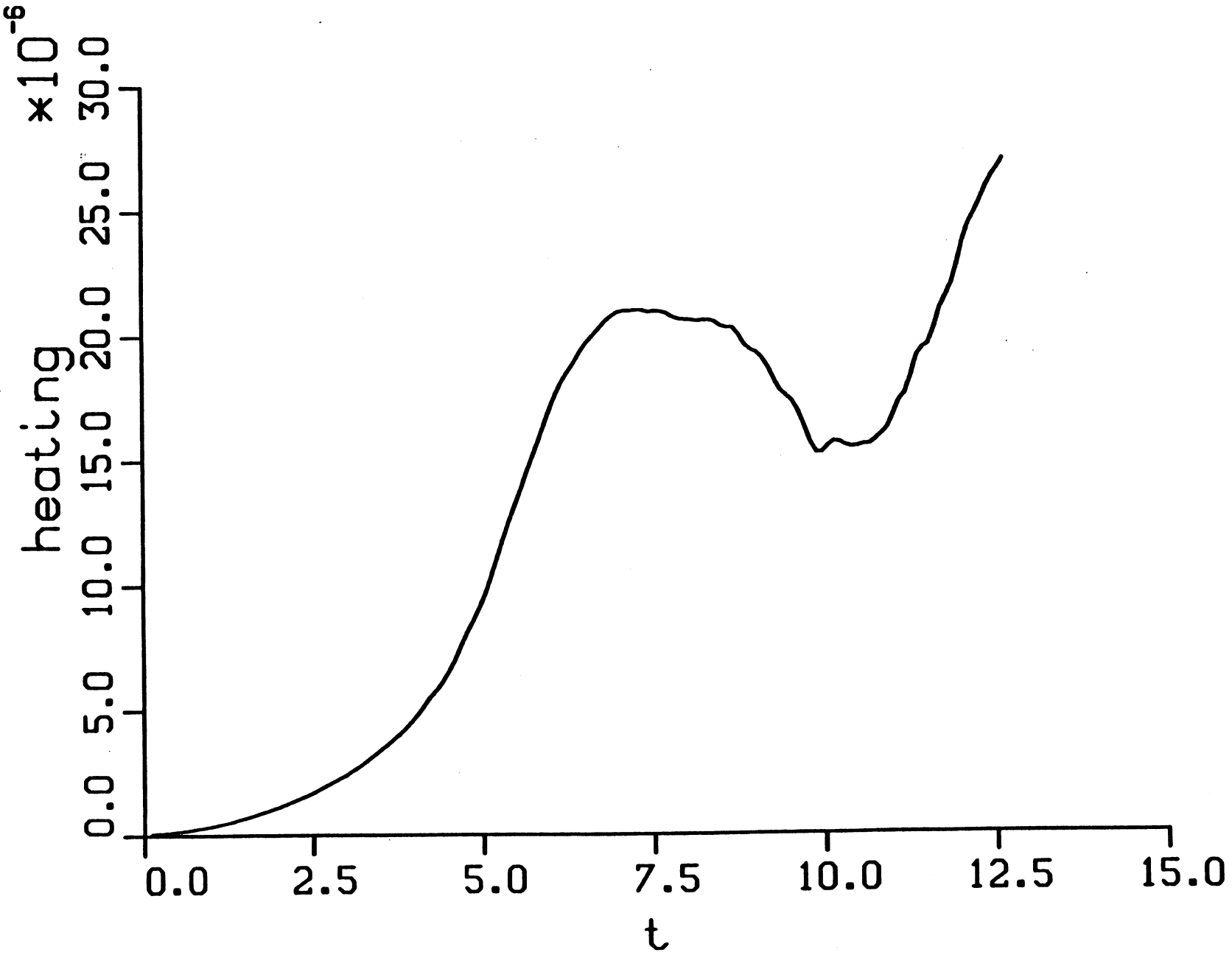

Figure 15

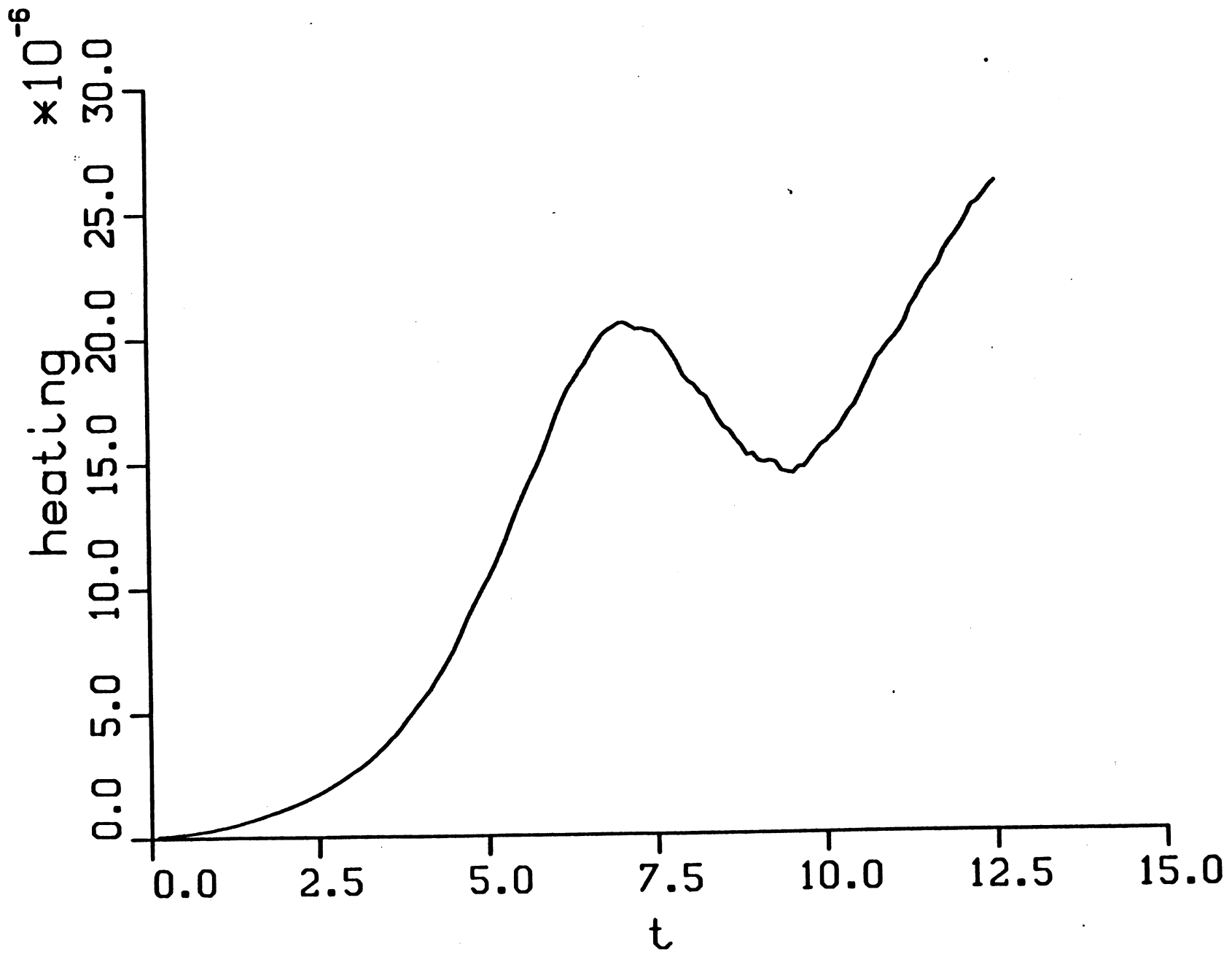

Fig 16

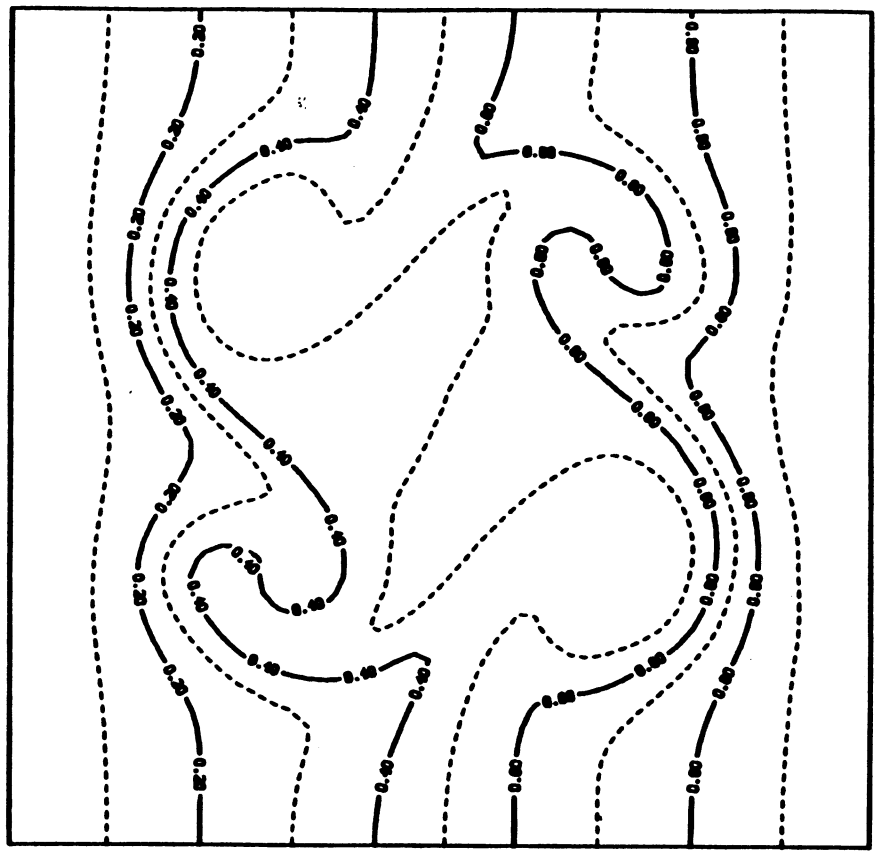

(A)

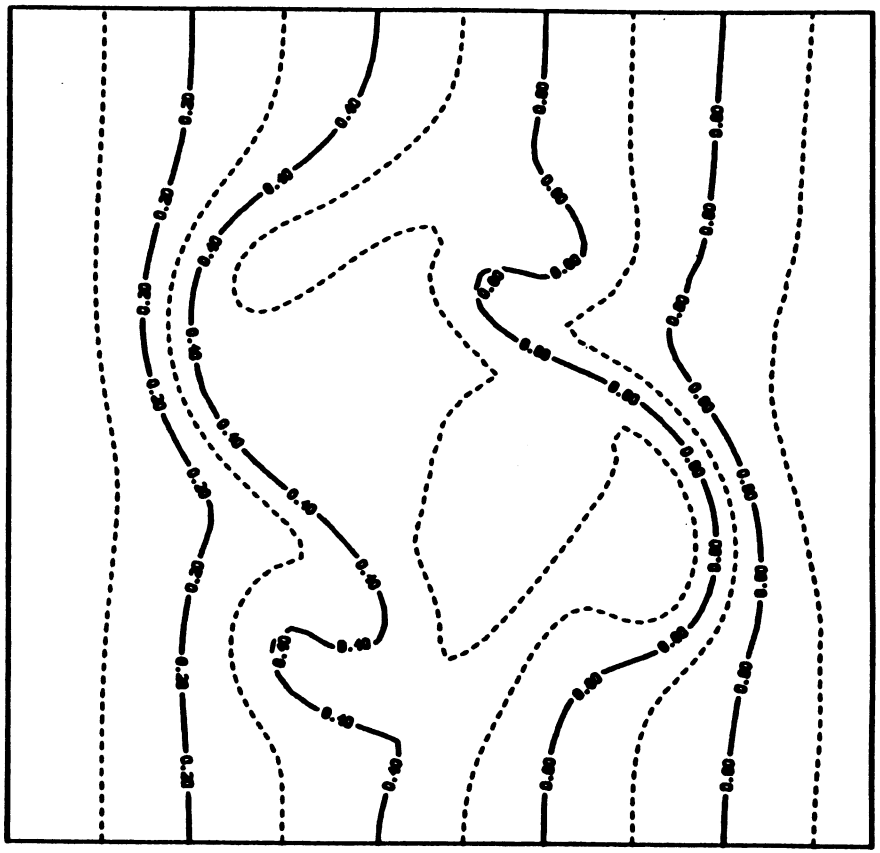

(B)

Fig. 17

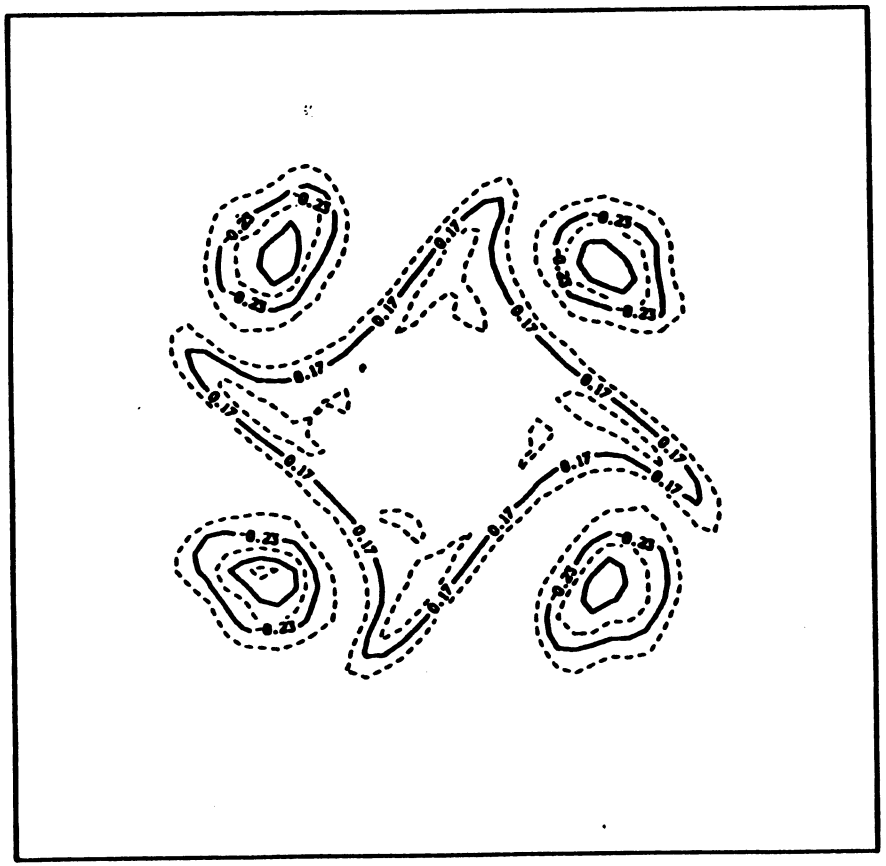

(A)

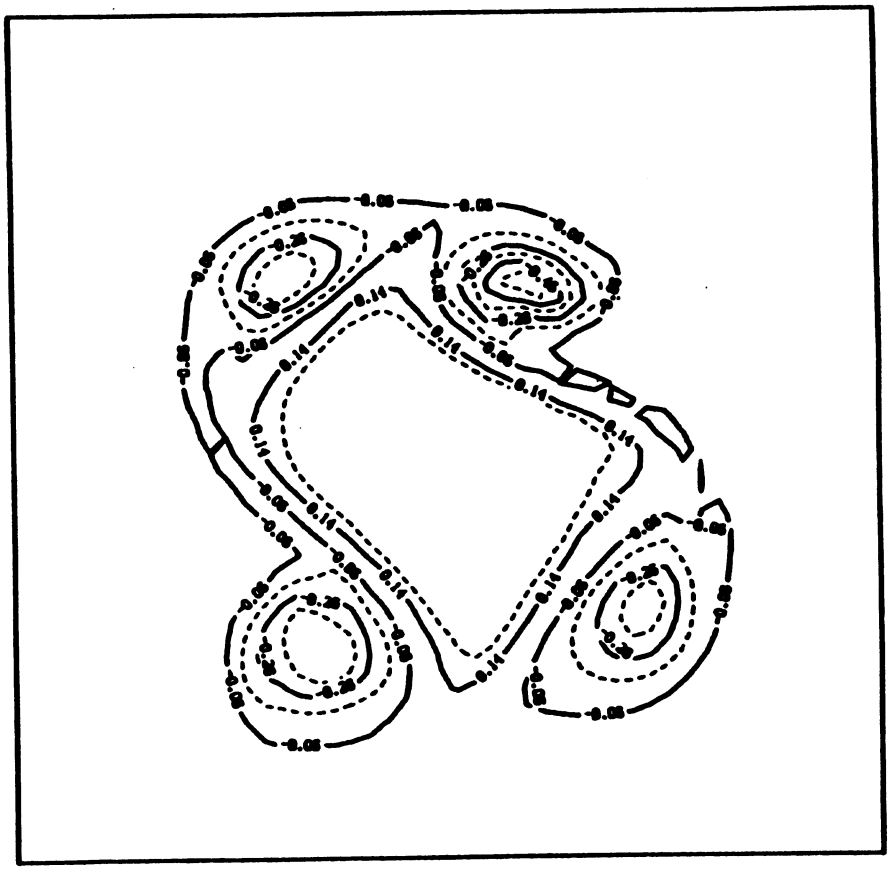

(B)

Figure 18

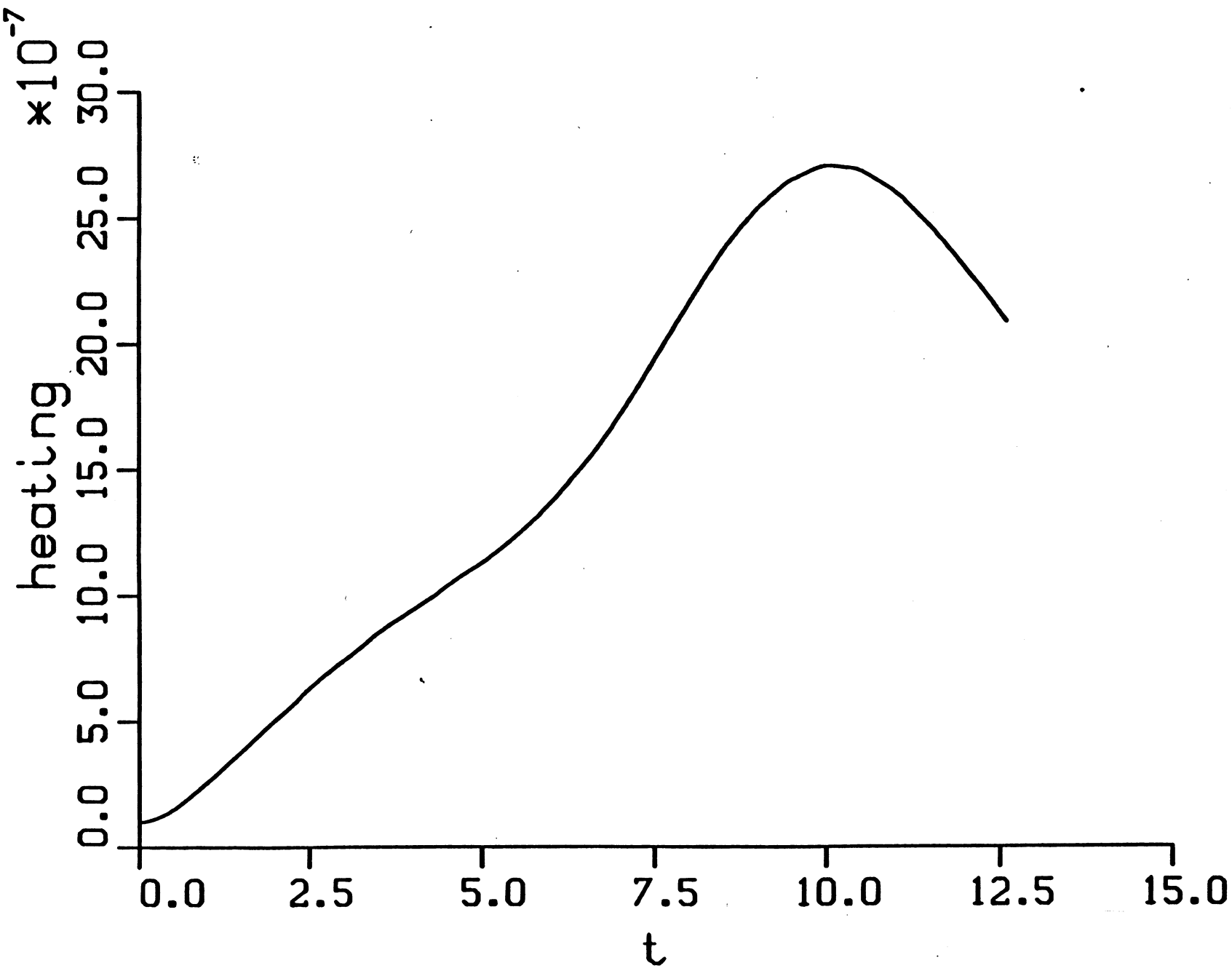

Figure 19